UNIVERSITY OF CALIFORNIA, MERCED

MODELING AND CONTROL OF AHUS IN BUILDING HVAC SYSTEM

by

Wei Liang

A thesis submitted in partial satisfaction of the
requirements for the degree of
Master of Science

in

Mechanical Engineering

Committee in charge:
Professor Jian-Qiao Sun, Chair
Professor YangQuan Chen
Professor Roummel Marcia

The thesis of Wei Liang is approved:

Jian-Qiao Sun, Chair Date

YangQuan Chen Date

Roummel Marcia Date

University of California, Merced

To my parents.

ACKNOWLEDGEMENTS

This thesis was completed by tremendous help from many other people and resources. I would like to express my deepest and earnest gratitude to my advisor, Professor Jian-Qiao Sun. I truly appreciate his patience and guidance to bring me from a yes man to an independent researcher. Dr. Sun's immense and profound knowledge, unwavering determination in the pursuit of knowledge, well-knit research style inspires me all the time. I will never forget when I first came to his office, he showed me his hand-drawing of the Hysteresis loop in 1980s. The tidy grids, the comprehensive equations explained the definition of "scholar" on my mind perfectly. I used to think that I would never have a chance to become a qualified college student, but Dr. Sun's endless support helps me return to the right path. I will always be grateful for his help in my life.

I would like to sincerely thank my thesis committee, Professor Roummel Marcia, and Professor YangQuan Chen for their time, expertise, insightful comments, and patience that significantly revised and enhanced this thesis. Thanks to Dr. Marcia for igniting my research interest in data science and optimization. Thanks to Dr. Chen, whose LinkedIn summary tells me the relationship between "working hard" and "working smart". He lets me know that tough is not enough; except working hard and following others' instruction, you need to work smart with your own creativity and try to be different. I will remember this principle in my future research career.

Great thanks are extended to UC Merced Facilities staffs, Dr. Varick Erickson, Mr. Zuhair Mased, and Mr. Julian Ho for helping our group, with promptness and care, obtain the web accesses to the HVAC control system and database, and providing insights into existing maintenance problems. Special thanks to Mr. Julian Ho, whose great patience and support help me build the HVAC engineering part of the thesis.

I would like to say thank you to the former member of our group, Siyu Wu, whose research provides the foundation of my research. I will also keep his intuitive understanding of independency on my mind. Special thanks to Mr. Xiaobao Jia for the help of mechanical drawings and his guidance of construction as an HVAC engineer, and Rebecca Quinte for the tremendous efforts for the review and revision of the thesis. And I am also grateful for my summer intern undergraduate students, Tammy Chan and Ramuel Safarkoolan for the work of collecting and pre-processing

the data. I would like thank to Yousef Sardahi for his help with the introduction part of this thesis.

I have been very privileged to get to know and work under the guidance from Mr. Joseph Deringer of Institute for the Sustainable Performance of Buildings and Dr. Xiufeng Pang of Lawrence Berkeley National Lab. Their technical skills, years of experience, and willpower to serve the community motivate me to chase my career goal on building energy efficiency.

I am enormously indebted to my friends, who share their joy, tears and advantures with me. I would like to thank Chuanjin Lan for inspiring me with his uncompromised determination in chasing career objectives; Shuo Liu and Youhong Zeng for their support during my last semester; Erik Levine for his kindness and help during my first year in Merced; Chengjie Qin and Zhengxian Qu for giving me strength and confidence in bodybuilding and basketball. I am also thankful to my classmates in Fuzhou No.1 Middle School, Xuan Jiang, Luyan Lin and Han Lu for their enthusiasm and sharing of new experiences. Special thanks to Shanjing Gu for her continuous support across the Atlantic ocean.

Last but not least, I would like to pay my heartfelt thanks to my families for their unconditional and unreserved love, trust, encouragement, and sacrifice. Especially, I want to thank my mother Xiaoli Liu, also a professional manager, for neutering me with morality, professionalism, and sense of justice; I want to thank my father Xiyi Liang for his endless support to this family. I am grateful for my maternal grandparents for raising me during my primary school years and the excellent example of professional ethics they provide as doctors. I want to thank my uncle Xuefeng Liu, and aunt Weihong Ren for the help when I was in Nanjing. I would like to thank my grandmother, whose diligence and courage inspire me to fight my laziness all the time.

Sincere gratitude to everyone who, helped me in their own way with this thesis.

CURRICULUM VITAE

Education

B.S. in Acoustics, Nanjing University (Nanjing, China), 2012.

Honors

Bobcat Fellowship (2014), University of California at Merced.
Summer Fellowship (2013), University of California at Merced.

TABLE OF CONTENTS

LIST OF FIGURES

LIST OF TABLES

ABSTRACT

Heating, ventilation and air conditioning (HVAC) is a mechanical system that provides thermal comfort and accepted indoor air quality often instrumented for large-scale buildings. The HVAC system takes a dominant portion of overall building energy consumption and accounts for 50% of the energy used in the U.S. commercial and residential buildings in 2012. The performance and energy saving of building HVAC systems can be significantly improved by the implementation of better and smarter control strategies. Therefore, it is of great benefits to developing automatic, intelligent, optimal and consistent model and control tools to ensure the normal operations of HVAC systems and increase the building energy efficiency.

Motivated by these goals, this thesis presents a parametric modeling approach and a system-level control design for HVAC systems. For the modeling, we establish dynamical models for return air for the air-handling-unit (AHU) of HVAC systems. The models include temperature and air flow rate models. These models follow the structure of the finite impulse response (FIR) model, and explicitly include the control variables from the AHU, the dynamical states, and the disturbances. Therefore, it is easy to apply this model to control design. Also, the model is flexible with prediction horizon and control horizon with a stability of the accuracy. In data processing, a convolution-based low-pass digital filter, Savitzky-Golay filter, and the Butterworth low-pass filter are used for data smoothing. As a result, the return air flow rate model becomes more feasible with the smoothed data.

Secondly, this thesis study develops a model predictive control (MPC) algorithm with the application of the dynamical models for AHU optimization problems. This control strategy optimizes the energy consumption of the AHU, and tracks the set points the room temperatures, supply air flow and return air flow rate of the building. The strategy provides physical-based inherent connection between components in AHU by applying damper positions, supply air temperature and outside air flow rate as manipulated variables. The control inputs are explicitly implemented into both the models and objective functions and the optimization structure is computationally efficient. The optimal results show an energy saving average percentage over 27.8% and track the supply air flow rate and set point of room temperatures in the building effectively. The thermal load, supply air flow rate set points are calculated from thirty-two VAVs, that ensures the internal cooling demand, the static pressure, and the ventilation level of the building.

In this thesis, all the data processing and modeling, model validation and implementation of the control algorithm are based on extensive data measurements collected from an office building on the campus of the University of California, at Merced. The control strategy is implemented into the online building automation system (BAS) of the building and can be easily incorporated with other BAS as well because of the explicit formulation.

Chapter 1

INTRODUCTION

1.1 Background

1.1.1 Building HVAC

Heating, ventilation, and air conditioning (HVAC) is a technology of indoor environmental comfort. HVAC is implemented for both residential and commercial buildings to maintain acceptable thermal comfort within reasonable installation, operation and maintenance costs.

Ever since the invention of its components during the industrial revolution, HVAC has gradually evolved into a highly interdisciplinary and complex system. Numerous new components, advanced sensing technologies, advanced control algorithms, and artificial intelligence have been introduced into HVAC to meet operational objectives in different types of buildings worldwide. Consequently, HVAC systems have been extensively deployed in both developed and developing countries. In the United States alone, HVAC systems condition a total area of nearly 3.1 billion square feet in buildings [1].

Due to increasing global population growth and civilization, more and more large-scale buildings are being built all over the world. Buildings have become one of the fastest growing energy consuming facilities on the earth. According to the U.S. Department of Energy's *2011 Building Energy Databook*, buildings use 74% of the nation's electricity, and 40.33% of the nation's total energy consumption which is valued at $431.1 billion [2–4]. HVAC systems make up almost 50% of the energy used in U.S. commercial and residential buildings [5]. Both organizations and governments put their efforts to reduce the energy consumption of HVAC systems. For example, the primary professional organization for regulation and standard of HVAC industry in the U.S., the American Society of Heating, Refrigerating and Air-Conditioning Engineers (ASHRAE), has published ASHRAE Standard 90.1 [6] to provide minimum requirements for energy efficient design for buildings including the HVAC part. And the application of the California Energy Commission's energy efficiency standards code title 24 has saved Californians more than $74 billion in reduced electricity since 1977 [7]. As such, bettering the efficiency of HVAC systems can significantly reduce the amount of electricity and energy buildings consume. The performance and energy saving of building HVAC systems can be significantly improved by the implementation of better and smarter control strategies.

1.1.2 Control of HVAC

As people's requirements of thermal comfort and energy efficiency increase, the development and implementation of effective control techniques for HVAC systems plays a major role in building energy management. Over the last decade, the cost of data processing, storage, and communication has decreased while the integration of building automation systems (BAS) has become more and more effective. It provides more possibilities for the design and implementation of state-of-the-art control techniques. Some conventional controllers, such as the on-off control and the proportional-integral-derivative (PID) control, are still commonly used in local HVAC system units [8,9] or single small building sections [10]. Although on-off control is the easiest to implement, its ability to control moving processes with nonlinear and time-delay dynamics is limited. In comparison, the PID control is effective but the parameter tuning is tedious. In order to track time-varying set points in HVAC systems, most research is focused on optimal tuning and auto-tuning approaches [11]; both can be time-consuming and disturb the normal operation [12].

"Hard control" is a controller design based on control theory, that has nothing to do with the word "hardware" [13]. It includes also PID control, nonlinear control, robust control, optimal control, adaptive control and MPC. For nonlinear controller design, typical approaches used are feedback linearization and adaptive control. He and Asada introduced feedback linearization to compensate for the nonlinearity of the evaporate dynamic system and implemented it in a PI controller design; although they found large estimation errors but they experienced successful results [14]. Moradi, Saffar-Avval and Bakhtiari-Nejad applied both gain-scheduling and feedback linearization techniques to manipulate the air-side and water-side valve position for better performance of indoor temperature and relative humidity on an air-handling-unit (AHU) [15], the same multi-input, multi-ouput (MIMO) unit considered by our approach. Since HVAC systems always have time-varying disturbances and tunable parameters, robust controllers are designed to fit these cumbersome properties. Wang and Xu developed a control strategy for AHU that uses freezing, gain scheduling, I-term reset, and linear transition control in combination with demand controlled ventilation and economizer control, thus solving instability problems in transitioning between different control modes and ensuring both indoor air quality (IAQ) and energy efficiency [16].

For HVAC systems, desired goals are to minimize energy consumption while optimizing thermal comfort. Therefore, researchers use optimal control to solve HVAC systems problems, which are treated as optimization problems to minimize a certain cost function. A system-level approach for optimizing multi-zone building systems is proposed by House and Smith [17]; it considers the interactive nature and parameters of HVAC systems in an effort to minimize system commissioning cost and energy consumption without sacrificing thermal comfort. Wang and Jin developed a supervisory controller using a search heuristic, Genetic Algorithm (GA)

optimization that mimics the natural selection, which led to considerable energy reduction in winter while improving IAQ in summer [18]. This strategy was based on predictions made using HVAC system dynamic models. Other evolutionary optimization algorithms like the particle swarm optimization algorithm (PSO), are also implemented in HVAC systems' prediction controls [19]. Among hard control approaches, model predictive control (MPC) is advantageous for HVAC systems since it works well with time-varing disturbance, nonlinear constraints, and slow-moving dynamics.

In contrast to hard control, the use of soft control has accelerated in recent years due to the development of digital control techniques and machine computation abilities. For example, fuzzy logic controllers use the if-then-else statement and follow intelligent rules; they are then incorporated into the auto-tuning of PID controller gains or considered with the trade-off between conflicted objectives, such as high demand for thermal comfort and reduction in energy consumption [20]. Also, the neural network (NN) is stimulated from biological neurons that connect input and output actions as a massively parallel distributed network, called the artificial neural network (ANN) [21]. This method is based on real data from the system and fits the nonlinearity of its dynamics, resulting in a black box modeling technique that eliminates the need to fully understand the underlying physics theory of the system process. The NN control design is often conducted by software-based simulation like TRNSYS [22, 23], Simulink and GenOpt. An example of NN control is a thermal comfort controller for AHU designed to the objective of predicted mean vote (PMV) by Liang and Du, considering six manipulated variables [24].

Additionally, the fusion of hard control and soft control results in hybrid controllers whose design implements soft control strategy at the higher levels of the system for a global mission and hard control techniques at the lower levels for accuracy and stability. A successful combination of these two control strategies can solve a problem which might not be fixed by one control applied individually. The fuzzy logic PID controller is a widely used application of hybrid control. A comparison between non-adaptive fuzzy PID, adaptive fuzzy PID, and conventional on-off control was proposed by Kolokotsa *et al.* The fuzzy controllers showed better satisfaction of thermal comfort and IAQ [25].

1.1.3 MPC for HVAC

The implementation of MPC into HVAC systems will be discussed in detail since the main control strategy considered in this thesis is MPC. MPC develops a system model to predict certain steps of the system's future state, and generates a corresponding control vector that minimizes the cost function within the prediction horizon. These systems might experience disturbances, which could be outside air temperature, unexpected overloaded occupancy thermal demand, constraints that might be caused by the rate and range limit of mechanical components, and physical

bound of manipulated variables. The first step of the computed control vector is applied to the plant while the remaining are discarded. This is repeated in the next time instant.

Since improvements in computers have lessened framework computational demands, MPC directs more and more attention to the building automation system (BAS). The number of papers devoted to MPC in the journals *Energy and Building*, *Building and Environment*, and *Applied Energy* has increased 100% in last twelve years [26]. Previous reviews have been done by Naidu and Rieger [13, 27], as well as Afram and Janabi-Sharifi [28]. Researchers design MPC using different objective functions to evaluate the performance of controllers. Samuel *et al.* combined a building thermal model with a weather-based control to maintain thermal comfort while minimizing energy consumption [29]. Maasoumy and Sangiovanni-Vincenteli focused on peak energy reduction by implementing an on-off controller and an MPC controller [30]. Morosan *et al.* considered temperature regulation, which reduced fluctuations from room set points [31]. Moreover, IAQ [32], energy performance in transient state [33], step response improvement [34], computation load reduction [31] and robustness of controlled system with disturbance [35] are also considered as objective functions in MPC design of HVAC problems.

Exciting results were found from both simulation and experimental sides of MPC application. The temperature regulation behavior and computational demand of decentralized, centralized and distributed MPC approaches are compared also with on-off and PI controls on a large-scale building with SIMBAD, a building and HVAC simulation toolbox for MATLAB and Simulink [31]. Maasoumy simulated the tracking and disturbance rejection results of MPC to a P controller, a tracking LQR control, and a modified LQR controller using Dymola, a commercial simulation interface of Modelica [36]. Experimental results also suggest the advantages in the use of MPC for HVAC system control. An experiment applying MPC to a building heating system was carried out on a real building in Prague, Czech Republic which showed an energy savings potential greater than 15% [29]. Rehrl and Horm compared the simulation and experimental results of both exact linearization and MPC, and the latter controller showed better tracking to future reference signal [37].

Details of MPC framework are discussed in Chapter 2.

1.1.4 Thermal Modeling

Mathematical models of HVAC components are used for detecting and diagnosing fault (fault detection and diagnosis, FDD), upgrading control strategies, and improving commissioning. A feasible model of HVAC systems can provide 20% to 30% energy savings [38]. Consequently, thermal modeling has been a very active field, attracting many researchers for the past two decades. Among all applications mentioned, models for controller design have been particular popularly since it is

difficult but valuable to have an accurate model fits the HVAC dynamic behavior to improve the control performance.

An HVAC system consists of different functional mechanical units, directly connects building sections, and works in conjunction with other building construction systems. Each part of the HVAC system (room, dehumidifier, heater, cooler, mixing chamber, fan and ductwork) can be described with mass and energy balance, and thermodynamic differential equations [39]. Otherwise, temperature models, especially room temperature models, are used as they characterize IAQ and thermal comfort, as is the case in the PMV model [40, 41], the ASHRAE Standard 55 [42], and the ISO Standard 7730 [43].

By generalization method, the thermal modeling can also be classified as physical-based models and data-driven models. Physical models are derived from the thermal and mechanical process. Model parameters can be fixed by manufacturer documentation and application of parameter estimation from measurement. Since thermal process is usually represented by first-order dynamic equations, analogous electrical RC network models are widely used. Wang and Xu developed and validated the lumped internal thermal parameters of building thermal network model using the genetic algorithm estimator using real data from site monitoring [44]. Thosar *et al.* implemented a zone temperature model to a feedback linearization VAV control developed from the energy transient equation [45], that achieved the desired performance even with large disturbances and changes in setpoints.

With the rapid development of data computation and storage abilities, data-driven models are more and more involved in prediction of HVAC system outputs (also called black box methods). Data-driven models work for both for linear and nonlinear mathematical functions to measure data. Examples of data-driven models include statistical models, for instance, auto-regressive (AR). Ríos-Moreno *et al.* demonstrated that the auto-regressive with exogenous (ARX) model can be adopted to predict classroom indoor air temperature with very high coefficients of determination. [46]. Yiu and Wang studied system identification of a multiple-input, multiple-output (MIMO) auto-regressive moving average exogenous (ARMAX) model to forecast the performance of an air conditioning system of an office building in Kowloon, Hong Kong [47]. Despite the above statistical methods, Mustafaraj *et al.* also compared other numerical models of room temperature in an office like output error (OE) and Box-Jenkins (BJ) model, and made a conclusion that the latter outperforms ARX and ARMAX [48]. For control application, researchers also use time delay models to represent HVAC system process. Bi *et al.* exploited relay plus step test determine the parameters of second order plus time delay model of air pressure loops and first order plus time delay model of air temperature loops and designed an auto-tuning PID controller for them. Other data-driven models, such as ANN [19], FL, support vector machine (SVM) [49] also come up with high accuracy but suffer from generalization capabilities [28].

It is natural to consider combining the strength of the physical-based model and the data-driven numerical approach. Wu and Sun proposed different multi-stage regression, physical-based linear parametric (mpbARMAX) models of room temperature and PMV index to take the advantage of both analytical and numerical modeling approaches. The multi-stage regression structure also reveals the relationship between the building thermal performance and the building parameters [50–53].

For MPC, the choice of thermal modeling also plays a key role in the whole control process. A detailed building model from building structure, mechanical components and material, might work effectively for subsystems by computer-aided modeling tools, i.e. TRNSYS [22] and EnergyPlus [54], and simulates and tracks the building system behavior. However, the implicity and complexity of the models reduce its possibility to implement with MPC strategy [26].

1.1.5 Air Economizer Control of AHU

The control problems in HVAC systems can also be classified from the structure side rather than methodology side. Over the last decade, there have been considerable research and development on model-based and optimal control algorithms for both HVAC equipments at the component level and system level. A complex HVAC system of a commercial building consists of cooling towers, chillers, AHUs, and zones with VAV units. Research on optimal control for cooling towers and chillers can be found in the work by Chow *et al.* [55] and Jin *et al.* [56] respectively. Within VAV, MPC approach by Huang [35] and GA optimization by Wang and Jin [18] are implemented.

Unlike other units, the AHU is multi-functional and nexus between central plant and building level of HVAC systems. An AHU is used to regulate, distribute, and recirculate air of an HVAC system. It includes different types of components, such as air dampers, fans, heating or cooling coils, humidifier, filters and mixing chamber. If an AHU uses 100% outside air and doesn't recirculate air, it is called a makeup air unit (MAU). Also, an AHU designed for outdoor use, usually on roofs, is known as a packaged unit (PU) or rooftop unit (RTU). Building Energy Systems Group of the Pacific Northwest National Laboratory (PNNL) estimated the energy and cost savings for RTUs from different control strategies individually and in combination using EnergyPlus for four building types in 16 locations covering all 15 climate zones in the U.S. [57]. Four control options, economizer control, fan speed control, cooling capacity control, and demand-controlled ventilation (DCV) were compared. The result showed that simply adding multi-speed fan control and DCV individually contribute the most to energy and cost saving for PUs.

As for typical AHUs, similar as control types mentioned from PNNL's work, fan control, cooling coil control, and air economizer control are applied. Bai *et al.* built a second-order plus dead-time plant representing the dynamics from the

supply fan variable speed drive to the supply air pressure, then implemented an auto-tuning PID controller on it [11]. The results demonstrated the superior performance of the auto-tuner over the manually tuned PID controller. With regard to cooling coil control, Wang *et al.* derived a simplified model from energy balance and heat transfer principles followed by parameter identification by either linear and nonlinear least square method [58]. The model is easy to apply to real-time cooling coil control since it contains the set points from the air side and the water side, and can serve as constraints in energy consumption optimization. Fong *et al.* implement an evolutionary programming technique in cooling coil control by optimizing both the set points of chilled water and supply air temperatures on a monthly basis, and achieved 7% saving potential compared to the one with the existing settings [59].

Last but not least, the air economizer takes in outside air to reduce mechanical cooling energy consumption and can be controlled easily by adjusting outside air damper, exhaust air damper, and recirculation air damper positions. The performance of an air economizer directly impacts on the electricity consumption of fans and cooling coil. Therefore, it has a great potential in energy and cost saving, and draws attention from researchers over the last two decades. Engineers in Johnson Controls presented a damper control system considering damper geometry, dynamic losses and pressure drop to prevent outside air entering the AHU through the exhaust duct [60]. Wang and Liu considered humidity control during an air economizer cycle to achieve IAQ requirements with a less energy price [61]. Yuan and Perez introduced MPC to the air economizer control with supply air temperature and outside air flow rate as control variables, that showed a cost effective performance compared to tradition PI controller [62]. Nassif and Moujaes developed a split-signal damper control theory [63]. The new operation strategy showed an annual energy saving and better fan performance compared to the conventional two-couple and three-coupled damper tuning approaches [64]. Seem and House simulated the model-based and the optimization-based control strategies to minimize cooling load by adjusting outside air fraction [65]. Wang and Song talked about derivative-based supply air flow rate and supply air temperature optimal control during an air economizer cycle in the case of MAU [66].

1.2 Our Approach

The pursuit of building energy efficiency and thermal comfort provides motivation for us to achieve a system-level modeling and control of HVAC system.

For the modeling, a parametric ARMAX model is presented for return air temperature and return air flow rate in an AHU. The resulting models take advantages of data-driven technique and are easy for control design implementation. As a result, the models fit the measurements pretty well and serve as the plant model in MPC algorithm with a flexibility of prediction horizon length.

For the control, a system-level MPC is designed for an HVAC system. By modeling the dynamics inside AHU and applying objectives and constraints from the lower level HVAC units, this control strategy links different levels of the HVAC system with a focus on energy consumption. Also, the computation load is low since the models and objective functions are explicit and the gradient inside this optimal control follows a fine structure. This control strategy reduces energy consumption meanwhile secure the enough cooling load, pressure balance, and thermal comfort of the building.

The rest of this thesis consists of four chapters. Chapter 2 presents the introduction of MPC, mathematical models commonly used in MPC, and a special MPC approach with Lagrangian Multiplier. Chapter 3 implements the ARMAX model of HVAC dynamics and MPC control with Lagrangian Multiplier to an HVAC system. Chapter 4 demonstrates the model validation and control simulation results based on data collected from a building on the campus of University of California (UC) at Merced. Finally, Chapter 5 summarize this thesis and take a look at the future work.

Chapter 2

REVIEW OF MPC

2.1 Introduction

In Chapter 1, we have discussed the application of MPC to HVAC systems. This chapter provides a review of mathematical principles and industrial applications of different MPC strategies and after that it focuses on the numerical method to solve the optimization problem arising from MPC, which is the Lagrangian approach.

Motivated by practical need from chemistry industries, the development of MPC has drawn a lot of attention from the control area academic community [67,68]. MPC is a thinking of control methodology rather than a specific control algorithm [69]. MPC predicts the future input and state from a dynamical model and optimization with respect to an objective function..

The basic methodology of MPC can be described as follows, and is shown in Figure 2.1:

1. The future predicted outputs $y_p(k+n \mid k)$, $n = 1, 2, \ldots, P$ are determined by the measurement information $y_m(k)$ up to the instant k and future control inputs $u(k+n \mid k)$, $n = 0, 1, \ldots, P-1$. The horizon P is called the prediction horizon. The expression $y_p(k+n \mid k)$ means the value is expected with the available information at instant k.

2. The set of future control inputs is calculated by an optimization based on an objective function. The criterion of the function usually takes the form of a quadratic function of the errors between the predicted outputs and the reference trajectory $y_r(k)$. For some specific MPC algorithms, like Model Algorithmic Control (MAC), the measurement value $y_m(k)$ is also taken into consideration to the tracking error. Constraints, linear or nonlinear, might be applied during the optimization.

3. The control input $u(k \mid k)$ is sent to the process while the remaining control signals in this series are discarded. At that time, the next sampling instant $y_m(k+1)$ is already known since the input has been updated. Then $u(k+1 \mid k+1)$ will be computed since the information at instant $k+1$ is available.

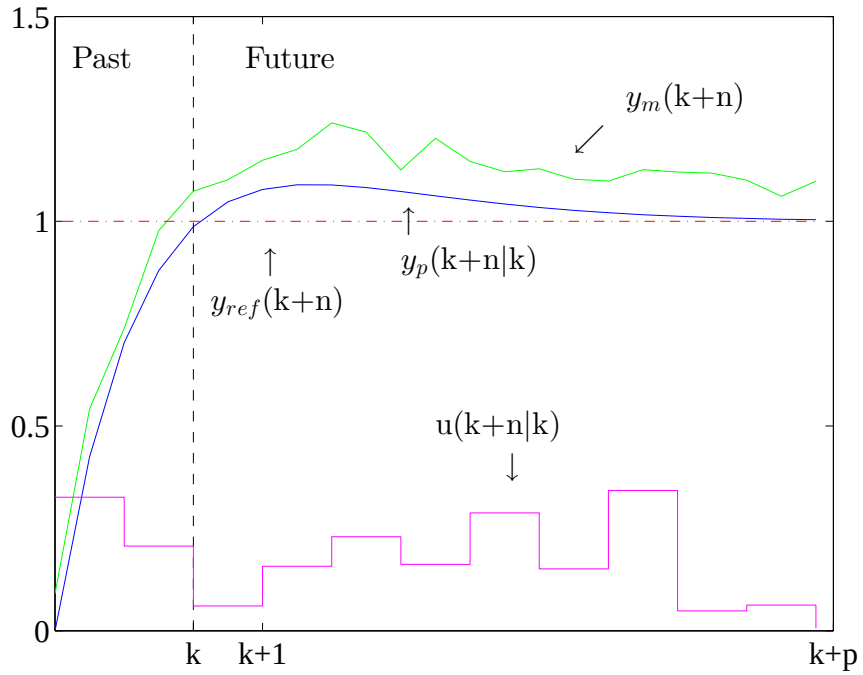

Figure 2.1: Example of elements in model predictive control: reference trajectory $y_{ref}(k+n)$, predicted output $y_p(k+n \mid k)$, measured output $y_m(k+n)$, and control input $u(k+n \mid k)$. $y_p(k+n \mid k)$ and $u(k+n \mid k)$ are expected values based on the information at instant k.

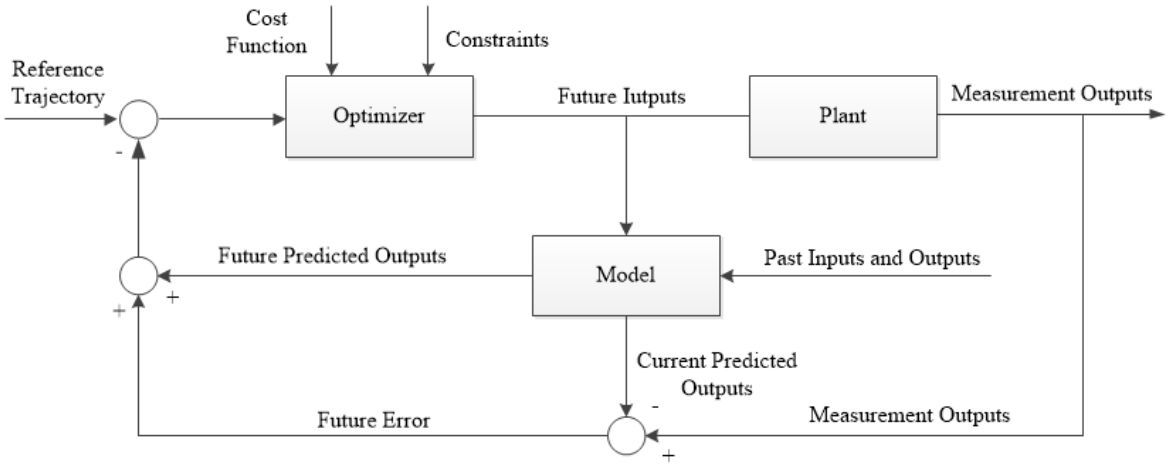

Figure 2.2: A typical diagram of MPC with measurement.

A basic structure of MPC is shown in Figure 2.2 with the current measurement correction included. A model is utilized to predict the future plant outputs based on past and current measurements of inputs and outputs. Considering the above information, the future control actions will be calculated by an optimizer with the cost function and constraints taken into account. From this figure, we can find out that the model plays a key role in MPC. Precision of the model is needed to mimic and predict the dynamical behavior of the real plant. In Section 2.2, we will introduce some candidates of process models of MPC in both academia and industry.

2.2 Process Models

The process model is one of the most basic elements in MPC. A comprehensive model should capture the process dynamics and assure the precision of prediction. Thus, it's important to choose the right models for various systems. Moreover, most MPC schemes were implemented with the development of digital computation. In our approach, the ARMAX model is used as the plant model of our MPC algorithm.

ARMAX models, used in statistical analysis of time series, are described in terms of three polynomials: an autoregressive (AR) part, a moving average (MA) part, and a series of exogenous (X) inputs:

$$y(k) = \sum_{i=0}^{N_P} a(i)y(k-i) + \sum_{i=0}^{N_C} b(i)u(k-i) + \sum_{i=0}^{N_D} c(i)w(k-i). \tag{2.1}$$

where $y(k-i)$ is the output sequence, $u(k-i)$ is the external inputs, and $w(k-i)$ is the disturbance. This model contains the states order N_P, the controls inputs order N_C, and the disturbance inputs order N_C, and coefficients $a(i), b(i), c(i)$ respectively. Typically they must be obtained by fitting the model to plant data. Obviously, $a(0) = b(0) = c(0) = 0$.

If there is no disturbance included, the model can be represented as

$$y(k) = \sum_{i=0}^{N_P} a(i)y(k-i) + \sum_{i=0}^{N_C} b(i)u(k-i). \tag{2.2}$$

This model is also called the Infinite Impulse Response (IIR) filter since it has an internal feedback to continue the impulse infinitely. Compared to Finite Impulse Response (FIR) filter, IIR filter meets a given set of specifications with a much lower filter order than a corresponding FIR filter. Moreover, the IIR filter contains the history of state error, which makes it trackable to the measurement noise, but needs to update online with a steep adaptation.

The IIR filter model is equivalent to different models, such as state space models and transfer functions [70]. Given the concept of state space in linear control theory, the model can be rewritten as a state space model

$$\begin{aligned} x(k) &= Ax(k-1) + Bu(k-1), \\ y(k) &= Cx(k). \end{aligned} \tag{2.3}$$

Similarly, if the time delay of control input is considered, the transfer function model can be shown as

$$y(z) = \frac{z^{-m}B(z^{-1})}{A(z^{-1})}u(z), \tag{2.4}$$

where $A(z^{-1})$ and $B(z^{-1})$ are polynomials of z-transform variable, m is the time delay. If $m = 0$, this model is equivalent to Equations 2.2 and 2.3. The parameter can be determined by experimental identification. However, to build this model, some prior knowledge should be considered such as the order of $A(z^{-1})$ and $B(z^{-1})$ [69]. This model is often used in Generalized Predictive Control (GPC), Unified Predictive Control (UPC) and Extended Prediction Self-Adaptive Control (EPSAC).

Moreover, if $a(i) = 0, i = 1, \ldots, N_P$ and $c(i) = 0, i = 1, \ldots, N_D$, the model can be described as the impulse response model, also called the finite convolution model. It represents the output by a weighted sequence of previous inputs at different time intervals. It appears in MAC. The relationship between output and input is given by

$$y(k) = \sum_{i=0}^{k} g(i)u(k-i). \tag{2.5}$$

This model is also known as the FIR filter. The response of an FIR filter to an impulse ultimately settles to zero because there is no feedback in the filter. The FIR filter can be written as the step response model

$$y(k) = \sum_{i=0}^{k} \beta(i) \Delta u(k-i), \tag{2.6}$$

where the parameter $\beta(i)$ known as the process step-response function; and $\Delta u(k-i) = u(k-i) - u(k-i-1)$. The step response model is commonly used in Dynamic Matrix Control (DMC) and its variants. It's easy to find its similarity to the impulse response model. They are equivalent [67] and connected as

$$g(i) = \beta(i) - \beta(i-1), \tag{2.7}$$

$$\beta(i) = \sum_{j=1}^{i} g(j). \tag{2.8}$$

To conclude, ARMAX model consists of the previous states, the control inputs and also disturbance. The properties ensure its ability to be adopted to MPC algorithm. Its equivalence to other models also provides the possibility to rebuild the model in different MPC strategy application and for different controller design objectives.

2.3 Lagrangian Solution Methods for Nonlinear MPC

The concept of Lagrangian Multiplier Methods stems from mathematical optimization for finding the local minima and maxima of a function subject to some equality constraints. The minimization of the optimization problem can be expressed as:

$$\min_{x \in D} f(x, y), \tag{2.9}$$

$$g(x, y) = c, \tag{2.10}$$

where $f(x, y)$ is the function needs optimization, subject to the constraint $g(x, y) = c$.

If $f(x, y)$ and $g(x, y)$ are continuous and first partial derivable, we can introduce a new variable λ as the Lagrangian Multiplier. The new objective is the Lagrange function defined by

$$L(x, y, \lambda) = f(x, y) + \lambda(g(x, y) - c), \tag{2.11}$$

The gradients of Lagrange function respective to x, y, λ can be derived as:

$$\begin{cases} \frac{\partial L}{\partial x} = \frac{\partial f}{\partial x} + \lambda \frac{\partial g}{\partial x}, \\ \frac{\partial L}{\partial y} = \frac{\partial f}{\partial y} + \lambda \frac{\partial g}{\partial y}, \\ \frac{\partial L}{\partial \lambda} = g(x, y). \end{cases} \tag{2.12}$$

The extremum is found by solving the 3 equations in 3 unknowns x, y, and the Lagrangian Multiplier λ. From Equation 2.12 it is easy to find that the gradient vectors of $f(x, y)$ and $g(x, y)$ are parallel, although their magnitudes are unequal. Note that the case $\lambda = 0$ is also a solution regardless of $g(x, y)$. If an extremum exists, the method of Lagrangian Multipliers yields a necessary and sufficient condition for optimality in this constrained problem [71]. This method is widely used in optimization problem equality constraints, but if Lagrangian Multipliers are nonnegative it also works for inequality constraints, which are also called as *Karush-Kuhn-Tucker conditions* (KKT) [72].

In control theory, the Lagrange Multiplier Method is often applied to form optimal controllers due to its flexibility to solve both lower and higher dimension constrained problems [73, 74]. A typical MPC scheme tries to solve a constrained optimization problem at discrete time steps whose decision variables are given as a control input sequence. The objective function is often in the formulation of linear quadratic regulation (LQR), which is easy to implement in Lagrange functions. Thus, an interactive way to compute the optimal manipulated variables is to use the Lagrangian Multipliers framework. A receding horizon, open-loop optimal MPC control law using Lagrangian Multipliers was introduced by Muske *et al.* [75]. The optimization problem is a nonlinear model with an equality constraint and an inequality constraint. Tøndel *et al.* converted a constrained linear MPC problem to a multi-parameter quadratic programming (QP) solver and found explicit MPC solution by applying KKT conditions [76]. Hovd utilized the calculation of 1-norm and infinite-norm of Lagrangian Multipliers of QP problems to design penalty functions for soft constraints in MPC [77]. Richter *et al.* discussed the certification of a fast gradient method obtained from the Lagrangian Multipliers Method and applied the certification procedure to a constrained MPC problem under KKT conditions [78]. Nedelcu and Necoara developed an approximate dual gradients method to update Lagrangian Multipliers and improved the number of iterations in a quadratic MPC problem [79]. All of these studies demonstrate that the Lagrangian Multiplier Method can be a good fit to solve MPC problems, especially for linear models, and satisfies both equality and inequality constraints.

The formulation of MPC with Lagrange Multipliers can be expressed as follows. In discrete time, a deterministic process control is

$$\begin{aligned} x(k+1) &= f(x(k), u(k)), \\ y(k) &= g(x(k)). \end{aligned} \tag{2.13}$$

These states $x(k)$ controls $u(k)$ and outputs $y(k)$ are vectors.

For a conventional MPC formulation, the objective can be written as

$$J = \sum_{j=0}^{N} (\Phi(y(k+j \mid k)) + Q_j \left| y_r(k+j) - y(k+j \mid k) \right|^2) \tag{2.14}$$
$$+ \sum_{j=0}^{N-1} R_j \left| \Delta u(k+j \mid k) \right|^2 .$$

This objective function contains a nonlinear objective term, the quadratic function of the tracking error to reference trajectory, the penalty of the control effort, where $Q_j, R_j > 0$ are the weights of each term. It should be noted that the objective function is calculated based on the prediction horizon and follows the form of summation. After introducing Lagrange Multiplier, the objective function can be expressed as

$$J^* = J + \sum_{j=1}^{N} \lambda_j (x(k+j \mid k) - f(x(k+j-1 \mid k), u(k+j-1 \mid k))). \tag{2.15}$$

Compared to the original equation 2.14, the Lagrangian term is added, where λ_j is the Lagrange Multiplier.

Therefore, the predictive controller solves at each time step the following optimization problem:

$$\min_{\mathbf{x},\mathbf{y},\mathbf{u}} J^*(\mathbf{x}, \mathbf{y}, \mathbf{u}, \lambda) \tag{2.16}$$

$$\text{s.t.} x(k+j \mid k) - f(x(k+j-1 \mid k), u(k+j-1 \mid k)), j = 1, \ldots, N, \tag{2.17a}$$
$$y(k+j \mid k) = g(x(k+j \mid k)), j = 0, \ldots, N-1, \tag{2.17b}$$
$$u(k+j \mid k) \in U, k = 0, \ldots, N-1, \tag{2.17c}$$
$$x(k+j \mid k) \in X, j = 1, \ldots, N, \tag{2.17d}$$

where U and X imply the bounds and constraints of control inputs and states. If the objective function is explicit to partial differentiation, we can find the gradient of J respect to all the variables:

$$\nabla J^* = \begin{bmatrix} \frac{\partial J^*}{\partial x(k+N|k)} \\ \frac{\partial J^*}{\partial x(k+N-1|k)} \\ \vdots \\ \frac{\partial J^*}{\partial x(k+1|k)} \\ \frac{\partial J^*}{\partial u(k+N-1|k)} \\ \vdots \\ \frac{\partial J^*}{\partial u(k|k)} \\ \frac{\partial J^*}{\partial \lambda_N} \\ \vdots \\ \frac{\partial J^*}{\partial \lambda_1} \end{bmatrix} = \mathbf{0}, \tag{2.18}$$

$$\begin{aligned} \mathbf{X} = [&x(k+N \mid k), x(k+N-1 \mid k) ... x(k+1 \mid k), \\ &u(k+N-1 \mid k), \dots u(k \mid k), \lambda_N \dots \lambda_1]^T. \end{aligned} \tag{2.19}$$

After solving 2.19 from the gradient 2.18, the optimal combination of future states, control inputs and Lagrange Multipliers can be found. The computational load is decided by the length of prediction horizon. The highlight of this method is introducing the dynamics of the system as a constraint inside the objective function, as the formulation of Lagrange Multiplier. Then the objective function turns to a Lagrange function.

Moreover, the structure of ∇J is also computational-friendly. For example, if $\Phi(y) = 0, y(k) = x(k)$, we rewrite $\nabla J^* = \mathbf{0}$ as $\mathbf{AX} = \mathbf{b}$,

$$\begin{bmatrix} 2Q_N & \mathbf{0} & \mathbf{I}_N \\ \mathbf{0} & \mathbf{R} & -\mathbf{B}^T \\ \mathbf{I}_N & \mathbf{B} & \mathbf{0} \end{bmatrix} \begin{bmatrix} x(k+N \mid k) \\ x(k+N-1 \mid k) \\ \vdots \\ x(k+1 \mid k) \\ u(k+N-1 \mid k) \\ \vdots \\ u(k \mid k) \\ \lambda_N \\ \vdots \\ \lambda_1 \end{bmatrix} = \mathbf{b}, \tag{2.20}$$

where the penalty matrix

$$\mathbf{R} = \begin{bmatrix} R_{N-1} & -R_{N-1} & & \\ & R_{N-2} & & \\ & & \ddots & \\ & & R_0 & R_0 \end{bmatrix}, \tag{2.21}$$

and the $N-1$ by N partial derivative matrix $\mathbf{B}$ with respect to control variables

$$\mathbf{B} = \begin{bmatrix} \frac{\partial f(x(k+N|k),u(k+N-1|k))}{\partial u(k+N-1|k)} & & \\ & \ddots & \\ & & \frac{\partial f(x(k+1|k),u(k|k))}{\partial u(k|k)} \end{bmatrix}. \tag{2.22}$$

After solving the linear system 2.20, the future control input array $\mathbf{U} = [u(k \mid k), \ldots, u(k+N-1 \mid k)]^T$ can be calculated.

For controls for HVAC systems, the Lagrange Multiplier is often used with physical-based and analytical models. Knabe and Felsmann designed an optimal operation schedule of HVAC systems based on Lagrange Multiplier method, and expressed the difficulties of its application in the technical field [80]. Marletta compared Lagrange Multipliers Method with the Monte Carlo method and Szargut-Tsatsaronis method, and discussed the possibility to use Lagrange Multipliers as sensitivity coefficients for HVAC systems' performance [81]. Chang chose the coefficient of performance (COP) of a chiller as the objective function, and adopted Lagrange Multiplier with the balance equation of the chiller's cooling load [82]; the experiment results on two building in Taipei showed a lower energy cost compared to the conventional control. As for the utilization of Lagrange Multiplier in the MPC strategy for HVAC systems, Kelman and Borrelli designed an MPC controller based on a dynamical model of AHUs with a strong assumption of thermal load in the building zone and outside air temperature [83]. In our approach, the Lagrange Multiplier is combined with the data-driven dynamical model in the objective function, which will be discussed in Chapter 3.

Chapter 3

MODELING AND CONTROL OF HVAC

3.1 Building Description

Extensive past and current measurements of the HVAC system in the Science and Engineering 1 (SE1) building of UC Merced are available to us. The network of sensors and controls for the HVAC system in SE1 building obeys the communication protocol for building automation and control networks (BACnet) by ASHRAE, ANSI and ISO standard [84]. The database and direct digital control (DDC) are accessible by an online building automation system, WebCTRL® [85], offered by Automated Logic. Such a highly instrumented building serves as an ideal living laboratory to support the research on energy efficiency.

For building geometry, the SE1 building is a four-floor, southwest orientation, $19,666$ gross square meter building with the primary use as office and laboratory. Two heating and cooling water bridges, nine unit heaters (UH), and ten air handling units (AHU) work together with sixty-one variable air volumes (VAV) to control and regulate 374 rooms and spaces in this building.

There are two major types of rooms, i.e., the faculty office and the conference room. The geometrical dimensions of the faculty office and the conference room are $3.2004 \times 4.4714 \times 3.0480$ (length$\times$width$\times$height) cubic meters, and $9.6012 \times 5.1816 \times 3.0480$ cubic meters, respectively. Figure 3.1 shows the third floor map of the SE1 building with detailed distribution of VAV units. Table 3.1 presents the geometries of the rooms regulated by VAVs under $AHU9$ ($A9$), which are responsible for the office space of the long wing side of the SE1 building. It should be noted that the volumes are calculated based on the room heights measured from the floor to the suspended ceiling. Some rooms have no surface exposed to the outside.

Merced, located in the San Joaquin Valley of California, is in the Mediterranean Steppe eco-region. Its climate exhibits rich variations during a given year. The summer is hot and dry from June to August, and the winter is cold and rainy from November to April. The measurements of the HVAC system have rich dynamics.

As for the central plant of the HVAC system on campus is a chilling plant containing a lead-lag-standby setup of three chillers, and the heating plant consists

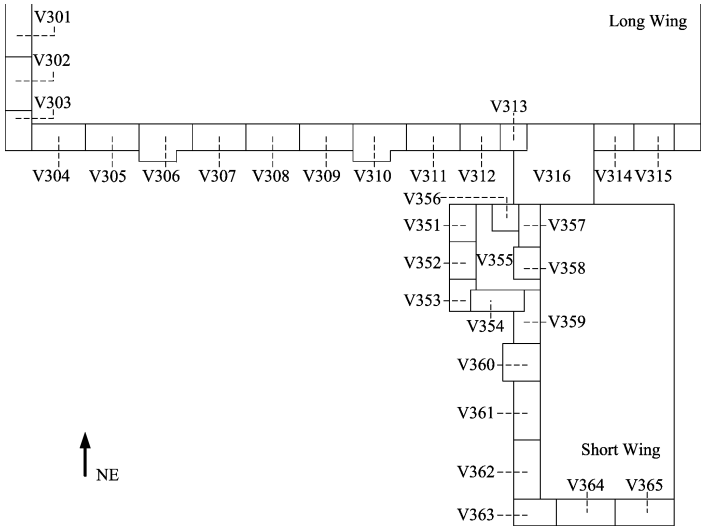

Figure 3.1: The distribution of VAVs on the third floor of the SE building on UC Merced's campus.

Table 3.1: The geometries of the rooms or spaces controlled by VAVs of AHU 9.

VAV	S_{wa} (m^2)	S_{wd} (m^2)	V (m^3)	VAV	S_{wa} (m^2)	S_{wd} (m^2)	V (m^3)
$V301$	0.4	46.8	170.0	$V201$	0.4	46.8	170.0
$V302$	4.8	24.5	167.4	$V202$	4.8	24.5	167.4
$V303$	8.8	30.4	124.9	$V203$	8.8	30.4	124.9
$V354$	19.0	10.2	131.0	$V204$	19.0	10.2	131.0
$V305$	19.0	10.2	131.0	$V205$	19.0	10.2	131.0
$V306$	19.3	52.1	315.2	$V206$	8.6	39.3	230.0
$V307$	19.0	10.2	131.0	$V207$	19.0	10.2	131.0
$V308$	19.0	10.2	131.0	$V208$	19.0	10.2	131.0
$V309$	19.0	10.2	141.3	$V209$	19.0	10.2	141.3
$V310$	19.3	52.1	431.4	$V210$	6.3	39.3	305.1
$V311$	19.0	10.2	131.0	$V211$	19.0	10.2	131.0
$V312$	12.7	6.8	87.3	$V212$	12.7	6.8	87.3
$V313$	6.4	3.4	75.5	$V213$	6.4	3.4	75.5
$V314$	12.7	6.8	87.3	$V214$	12.7	6.8	87.3
$V315$	12.7	6.8	90.4	$V215$	12.7	6.8	90.4
$V316$	20.8	94.18	989.0	$V216$	6.3	94.18	618.1

of three, dual fuel boilers. The pump speeds of both plants are modulated by PID controls to maintain differential pressures at discharge. To building level subsystems, the AHU units apply logic and PID controls to regulate the supply fan variable-frequency drive (VFD), return fan VFD, adjust the damper position of chilling water and supply air temperature. These control loops maintain the duct pressure, return fan discharge pressure, and supply air temperature according to the set point. The VAV units implement two separate control loops, i.e., the cooling loop and the heating loop, to keep the temperature at set point. Both of the loops apply PI controls with three operational modes: heating, cooling, and deadband. In summer, the heating loop is barely used and the cooling valve is always open.

The PID controls are localized and are actually involved in one another by thermodynamics. However, the relationship of the inputs, outputs, parameters, and disturbance of each control loop are not explicit from WebCTRL®. Thus, for a more global and intelligent control strategy, we need to build dynamical models for this HVAC process.

3.2 Mathematical Model

3.2.1 Introduction

Commercial buildings in the education sector, like the SE1 building, need commissioning all the year round. Figure 3.2 shows the schematic diagram of an AHU in the SE1 building. It's a single duct AHU which means the supply air uses only one duct for supply air (SA) under both cooling and heating mode. The AHU has two inputs, the outside air (OA) and the return air (RA), and two outputs, the supply air and the exhaust air (EA). The supply fan and return fan modulate the variable frequency drive (VFD) to provide the pressure difference and three dampers (outside air damper, exhaust air damper, and recirculation air damper) control the air flow rates between the AHU and outdoors. The chiller in the supply duct maintains the supply air temperature set point. All the components, chiller, dampers, fans, and VFDs are controlled to achieve the goal, providing cooling load to the office space of SE1 building.

3.2.2 Return Air Dynamical Model

The process can be expressed by Figure 3.3. This loop can be divided by the following procedure:

1. AHU mixing and cooling

   In the AHU process, part of the return air from the building is mixed with outside air in the mixing chamber. After that, the mixed air (MA) goes through filters driven by supply fan. The temperature of the air will be typically cooled to 55 F (13°C) and supplied to the VAVs. The ratio of the return air recycled

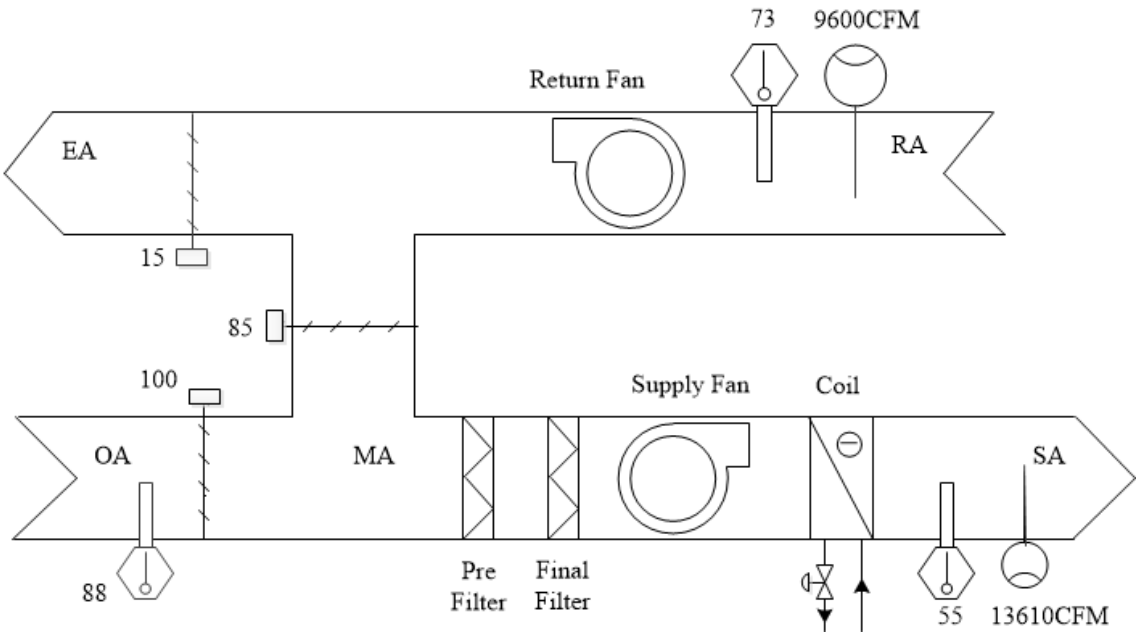

Figure 3.2: A typical single duct air handling unit.

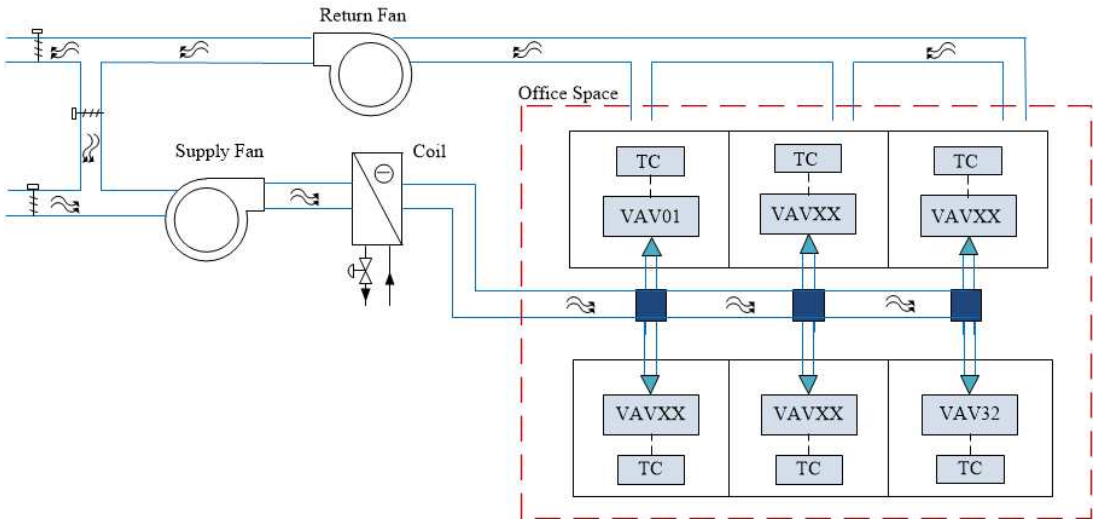

Figure 3.3: The air recirculation loop of $AHU9$.

can be determined by the damper position of the exhaust air damper and the return air damper, which is

$$\beta = \frac{D_{RA}}{D_{EA} + D_{RA}}. \tag{3.1}$$

2. Duct distribution to VAVs

   The VAVs distribute the supply air to different building zones. Reheating might be included in the VAVs during fall and winter time. Passing duct work and diffusers, the temperature of discharge air (DA) to different rooms varies from each other and the supply temperature.

3. Room thermal loading and air returning duct work

   After serving the rooms, the HVAC system also collects room air from office space to recirculate, keep ventilation, and meet thermal comfort. The real time room air from $VAV201-216$ and $VAV301-316$ will be collected by the return fan of $AHU9$ from return air duct in each room. Then the return air will participate in the recirculation loop of the next time span. This process can be mathematically represented by

$$\begin{aligned} T_{RA} &= \sum_{i=1}^{32} \rho_i T_{z,i}, \\ \rho_i &= \frac{V_{z,i}}{\sum_{i=1}^{32} V_{z,i}}. \end{aligned} \tag{3.2}$$

where $T_{z,i}$ is the zone temperature served by the ith VAV, $V_{z,i}$ is the volume of each room, and ρ_i is the relative weight of each room. Obviously, $\sum_{i=1}^{32} \rho_i = 1$.

Therefore, the top-down level of the HVAC system in the SE1 building is connected by this air recirculation loop. From the process, we can find that the return air can be considered as an output as well as the feedback of this loop. Hence, the return air temperature and return air flow rate can be used as two states of our mathematical model. Both of them are affected by the recirculation air damper ratio β, supply air temperature T_{SA}, outside air flow rate $\dot{m}_{OA}$, outside temperature T_{OA}, the states of themselves before, and the discharge flow rate, as well as the room temperature setpoint of each room. Details will be provided in Section 3.3 From Equation (3.2) we can find that return air temperature is a reference of the

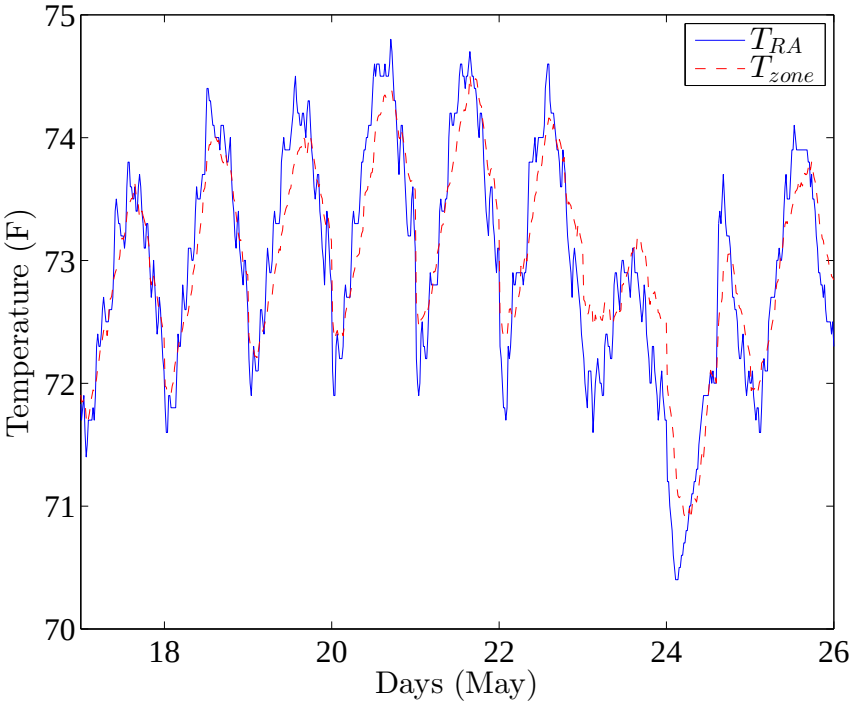

Figure 3.4: Mathematically equivalent measurements show a very high correlation between the calculated air from the VAVs and the return air temperature measurements from $AHU9$.

room temperature measurements. To confirm that, the calculated T_{RA} from room temperature measurements of $VAV201-216$ and $VAV301-316$ are compared with the return air temperature of $AHU9$. The data is collected from 7 days of May, 2014. Figure 3.4 show that they track each other very well. A further correlation analysis shows that the correlation coefficient between them is 0.9478.

As for the return air flow rate, it is proportional to the supply air flow rate to the office space to maintain both the thermal and ventilation balance. The ratio changes with the time partition but is steady in a certain time span. An equivalent connection also needs to build across the top-down hierarchy. We also provide a validation example for this relative reference. We track the measurements of discharge air flow of each VAV units and the return air flow rate of $AHU9$ during the same time as the validation of return air temperature. Figure 3.5 shows the mathematical equivalence of the summation of the discharge flow rate and the supply air of $AHU9$ with a correlation coefficient of 0.9561. That means $AHU9$ adjusts the supply air flow rate according to the demand of the office space.

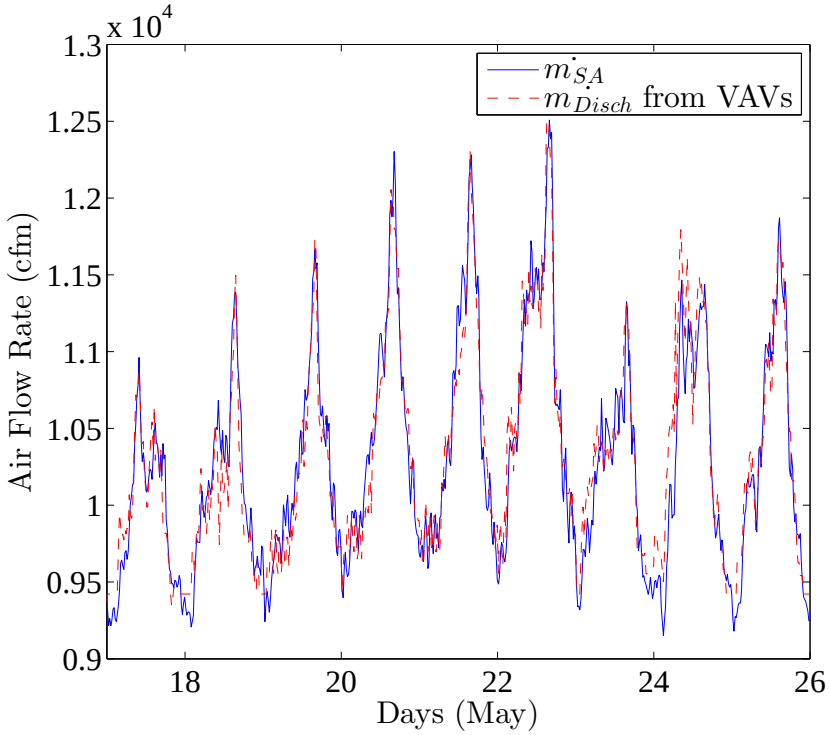

Figure 3.5: Mathematically equivalent measurements show a very high correlation between the discharge air flow rate from VAVs and the supply air flow rate measurements from $AHU9$

Now we can try to derive the mathematical model from the HVAC background. Typically a first order plus time delay (FOPTD) is used to represent an HVAC process [86] such as

$$G(s) = \frac{X(s)}{U(s)} = \frac{K}{Ts+1}\exp(-Ls), \tag{3.3}$$

where K is the process gain and L represents the time-delay. The input and output logged until the process enters a new steady state gain. The parameter identification of this model is easy but might be sensitive to measurement noise and determined by complex manipulated variables. Additionally, FOPTD works better for components rather than a multi-agent process. For multiple control inputs and state variables, and systems with disturbance, we consider the ARMAX model

$$x(n+1) = \sum_{i=0}^{N_P} a(i)x(n-i) + \sum_{i=0}^{N_C} b(i)u(n-i) + cw(n), \tag{3.4}$$

where $x(n)$ is the state variable,$u(n)$ is the control input and $w(n)$ is the disturbance. The model is explicit for control design. Take the return air temperature model as an example:

$$\begin{aligned} T_{RA}(n+1) = &\sum_{i=0}^{N_P} a_t(i)T_{RA}(n-i) + \sum_{i=0}^{N_C}(b_{t,1}(i)\beta(n-i) + b_{t,2}(i)T_{SA}(n-i) \\ &+ b_{t,3}(i)\dot{m}_{OA}(n-i)) + c_t T_{OA}(n). \end{aligned} \tag{3.5}$$

This model is easy to implement into a controller design. T_{RA} is the state being observed, β, $T_{SA}(n-i)$ and $\dot{m}_{OA}$ are manipulated variables, and T_{OA} represents the real time climate treated as a disturbance since it cannot be controlled. Large scale of measurements from AHU, VAVs, and outside air condition are available to determine the model parameters. This results in a collection of coefficients $\mathbf{a}_t$, $\mathbf{b}_{t,1}$, $\mathbf{b}_{t,2}$,$\mathbf{b}_{t,3}$ and c_t. It should be noted that when the length of the prediction horizion is 1 or 2, the order of this ARMAX model is consistent with the thermodynamic laws.

3.2.3 Energy Model

The energy consumption of an AHU in Figure 3.2 consists mainly of the cooling load of the water chiller and electricity usage of both the supply fan and the return fan.

$$\begin{aligned} En_{AHU} &= En_{CW} + W_F t, \\ W_F &= W_{SF} + W_{RF}. \end{aligned} \tag{3.6}$$

The water coil needs to cover the energy required to cool down mixed air to the set point of the supply air temperature. It is assumed and so it is in Merced that the outside air is very dry, where the dew point is less than 55 F (13C). That means no latent heat is lost and only the sensible cooling load is considered during the cooling process. In the continuity condition, $\dot{m}_{MA} = \dot{m}_{SA}$, therefore the energy consumption of the water chiller can be expressed as

$$En_{CW} = c_p \dot{m}_{SA}(T_{MA} - T_{SA}). \tag{3.7}$$

Before passing through the supply fan, the mixed air temperature is fixed by the combination of outside air and recirculated air in the mixing chamber. If T_{MA} is above saturation line, the moisture in the air won't condensate, and the flow rate and temperature balance during an air economizer cycle is

$$\dot{m}_{SA} = \dot{m}_{OA} + \beta \dot{m}_{RA}, \tag{3.8}$$

$$c_p \dot{m}_{OA} T_{OA} + \beta c_p \dot{m}_{RA} T_{RA} = c_p \dot{m}_{SA} T_{MA}. \tag{3.9}$$

Combining Equation (3.7), (3.8) and (3.9), the cooling load can be expressed as

$$\begin{aligned} En_{CW} &= c_p \dot{m}_{SA} T_{MA} - c_p \dot{m}_{SA} T_{SA}, \\ &= c_p \dot{m}_{OA} T_{OA} + \beta c_p \dot{m}_{RA} T_{RA} - c_p(\dot{m}_{OA} + \beta \dot{m}_{RA}) T_{SA}, \\ &= c_p \dot{m}_{OA}(T_{OA} - T_{SA}) + \beta c_p \dot{m}_{RA}(T_{RA} - T_{SA}). \end{aligned} \tag{3.10}$$

Otherwise, the power usage of the supply and return fans follows the affinity law. P is proportional to the third power of the flow rate $\dot{m}$, as shown in Equation (3.11).

$$\begin{aligned} W_F &= W_{SF} + W_{RF}, \\ &= W_{SF,ref}(\frac{\dot{m}_{SA}}{\dot{m}_{SA,ref}})^3 + W_{RF}, ref(\frac{\dot{m}_{RA}}{\dot{m}_{RA,ref}})^3. \end{aligned} \tag{3.11}$$

The reference power and flow rate are calculated from real operation of HVAC system in the SE1 building.

In summary, the energy consumption of AHU can be expressed as

$$\begin{aligned} En_{AHU} = c_p \dot{m}_{OA}(T_{OA} - T_{SA}) + \beta c_p \dot{m}_{RA}(T_{RA} - T_{SA}) \\ + W_{SF,ref}(\frac{\dot{m}_{SA}}{\dot{m}_{SA,ref}})^3 + W_{RF,ref}(\frac{\dot{m}_{RA}}{\dot{m}_{RA,ref}})^3. \end{aligned} \tag{3.12}$$

3.3 Control Formulation

3.3.1 HVAC Background

A stereotype AHU is multi-functional. The primary purposes include distribution of supply air to the building zone at a set point value, keeping the building in static pressure. As described in Section 3.2.2, $AHU9$ in the SE1 building is running in an enconomizer cycle, and the transient time is short compared to the steady state of each time span. For dampers, the outside air flow rate, and the supply air temperature, local PID control is applied to every single component with only a simple link to each other [12]. However, to minimize energy consumption and optimize thermal comfort, the traditional control might not yield the optimal solution. In this section, an energy efficient and multi-objective MPC control strategy that considers ventilation and thermal load is introduced based on the same control variables in the original local PID control. The advantages of applying MPC include:

- A physical-based inherent connection between components in the AHU, and considers cross-level constraints in the whole HVAC system of the SE1 building.
- The controller is designed to be online, receding state prediction and future optimal control inputs calculation.
- The impact of measurement noise and nonlinearities is reduced by data regression and time domain integration.
- The algorithm is based on WebCTRL®, and is easily implemented into building automation systems.

3.3.2 Model Predictive Control

For comparison, the same manipulated variables are chosen as the original local PID control: the recirculation air damper ratio β, the supply air temperature T_{SA} and the outside air flow rate $\dot{m}_{OA}$. The model of $AHU9$ in the SE1 building includes the control inputs and can be represented by the model proposed in Section 3.2.2. For simplicity, the prediction horizon is set to be N and the control horizon is used as $N-1$:

$$\mathbf{x}(k+1) = \sum_{i=0}^{N} \mathbf{A}(i)\mathbf{x}(k-i) + \sum_{i=0}^{N-1} \mathbf{B}(i)\mathbf{u}(k-i) + \mathbf{C}w(k), \tag{3.13}$$

where $\mathbf{x}(k) = [T_{RA}(k), \dot{m}_{RA}(k)]^T$, $\mathbf{u}(k) = [\beta(k), T_{SA}(k), \dot{m}_{OA}(k)]^T$, $w(k) = T_{OA}(k)$. Note that $\Delta\mathbf{u}(k) = [\Delta\beta(k), \Delta T_{SA}(k), \Delta\dot{m}_{OA}(k)]^T$, rather than $\mathbf{u}(k)$, is commonly calculated in realistic computation, and $\Delta\mathbf{u}(k) = \mathbf{u}(k) - \mathbf{u}(k-1)$.

Then the objective function can be expressed at every sample time k:

$$
\begin{aligned}
J = \sum_{j=0}^{N} & (Q_{1j} \left| T_{RA,ref}(k+j) - T_{RA}(k+j \mid k) \right|^2 \\
& + Q_{2j} \left| \dot{m}_{RA,ref}(k+j) - \dot{m}_{RA}(k+j \mid k) \right|^2) \\
& + \sum_{j=0}^{N-1} (En_{AHU}(k+j \mid k) + Q_{3j} \left| \dot{m}_{SA,ref}(k+j) - \dot{m}_{SA}(k+j \mid k) \right|^2 \\
& + R_{1j} \left| \Delta\beta(k+j \mid k) \right|^2 + R_{2j} \left| \Delta T_{SA}(k+j \mid k) \right|^2 \\
& + R_{3j} \left| \Delta\dot{m}_{OA}(k+j \mid k) \right|^2),
\end{aligned} \tag{3.14}
$$

where $En_{AHU}(k)$ follows the structure of Equation (3.12), $T_{RA,ref}(k)$ and $\dot{m}_{RA,ref}(k)$ is the designed set point from historic data as reference of zone temperature and ventilation level of SE1 building It should be noted that the supply air flow rate $\dot{m}_{SA,ref}(k)$ is also an observable variable. It indicates the demands of fresh air amount. Also, its product multiplying to $T_{RA,ref}(k)$, the reference of the room temperatures set point, can present cooling load demand of the building. The supply air flow rate $\dot{m}_{SA,ref}(k)$ can be represented as Equation (3.8).

To find optimal control inputs, the gradient-based Lagrangian solution method are introduced to the objective function. The mathematical models of the states $T_{RA}(k)$ and $\dot{m}_{RA}(k)$ serve as constraints of the dynamical behavior of HVAC system. They are linked to the original objective function with Lagrangian Multipliers. Thus, the updated objective function can be defined as:

$$
\begin{aligned}
J^* = J + \sum_{j=1}^{N} & \lambda_j (T_{RA}(k+j \mid k) - f(T_{RA}(k+j-1 \mid k), \Delta\mathbf{u}(k+j-1 \mid k))) \\
& + \mu_j (\dot{m}_{RA}(k+j \mid k) - g(\dot{m}_{RA}(k+j-1 \mid k), \Delta\mathbf{u}(k+j-1 \mid k))).
\end{aligned} \tag{3.15}
$$

where $f(T_{RA}(k+j-1 \mid k), \Delta\mathbf{u}(k+j-1 \mid k))$ and $g(\dot{m}_{RA}(k+j-1 \mid k), \Delta\mathbf{u}(k+j-1 \mid k))$ are referred to the ARMAX models in Equation 3.13.

The optimization problem is shown from Equations (3.16) to (3.17g):

$$
\min_{\Delta\mathbf{u}} J^*(\mathbf{x}, \Delta\mathbf{u}, \lambda, \mu), \tag{3.16}
$$

subject to the following constraints:

$$\beta_{\min} \leq \beta(k+j \mid k) \leq \beta_{\max}, \tag{3.17a}$$
$$T_{SA,\min} \leq T_{SA}(k+j \mid k) \leq T_{SA,\max}, \tag{3.17b}$$
$$\dot{m}_{OA,\min} \leq \dot{m}_{OA}(k+j \mid k) \leq \dot{m}_{OA,\max}, \tag{3.17c}$$
$$\Delta\beta_{\min} \leq \Delta\beta(k+j \mid k) \leq \Delta\beta_{\max}, \tag{3.17d}$$
$$\Delta T_{SA,\min} \leq \Delta T_{SA}(k+j \mid k) \leq \Delta T_{SA,\max}, \tag{3.17e}$$
$$\Delta\dot{m}_{OA,\min} \leq \Delta\dot{m}_{OA}(k+j \mid k) \leq \Delta\dot{m}_{OA,\max}, \tag{3.17f}$$

$$T_{RA}(k+j \mid k) = f(T_{RA}(k+j-1 \mid k), \Delta\mathbf{u}(k+j-1 \mid k)), \tag{3.17g}$$
$$\dot{m}_{RA}(k+j \mid k) = g(\dot{m}_{RA}(k+j-1 \mid k), \Delta\mathbf{u}(k+j-1 \mid k)). \tag{3.17h}$$

The control inputs in this study have different physical meanings. β is the recirculation air damper ratio; it is easy to find if the return air damper is fully open ($D_{RA} = 1$) and the exhaust air damper is fully closed ($D_{EA} = 0$) at the same time. When this occurs $\beta = 1$, which means all the return air is recycled for the next time span of air supply. Otherwise, when the return air damper is fully closed ($D_{RA} = 0$) and the exhaust air damper is fully open ($D_{EA} = 1$), $\beta = 0$. In this situation, the return air is all relieved and the supply air is provided by fresh air. However, to keep the building static pressure's balanced and make sure there is enough fresh air for supply, these two extreme cases would not happen. The physical lower bound of D_{EA} and D_{RA} is set to 15% and 12% respectively. The upper bounds are both 100%, fully open. Therefore the range of β can be shown as:

$$\begin{aligned} \beta_{\min} &= \frac{D_{RA,\min}}{D_{EA,\max} + D_{RA,\min}} \approx 11\%, \\ \beta_{\max} &= \frac{D_{RA,\max}}{D_{EA,\min} + D_{RA,\max}} \approx 87\%. \end{aligned} \tag{3.18}$$

To determine the bounds of T_{SA}, the designed supply air temperature $T_{SA,d}$ of 55 F (13 C) is used as the lower bound $T_{SA,\min}$. This is a conventional temperature for supply air in HVAC systems. However, if the dew point of the outside air is below 55 F, the latent cooling load would not exist. In this case, no saturated steam will condensate [66]. Therefore the T_{SA} can be not limited and higher set point can be used for reducing the AHU's energy consumption. It should be noted that $T_{SA,\max}$ is cooling load demand generated by occupants and devices in the building zone area.

For the outside air flow rate $\dot{m}_{OA}$, the minimum outside air flow rate is 3000 cubic feet per minute (cfm), which is determined by the BAS of the SE1 building.

This number is set according to the requirement of the outdoor air needed per person in office buildings from ASHRAE Standard 62.1 [87]. The upper bound value of the outside air flow rate cannot exceed that of the supply air flow rate. The limitations of $\dot{m}_{OA}$ can be shown as:

$$\begin{aligned} \dot{m}_{OA,\min} &= 3000 \text{ cfm}, \\ \dot{m}_{OA,\max} &= \dot{m}_{SA,d}. \end{aligned} \tag{3.19}$$

In addition, the reference trajectory in this approach, $T_{RA,ref}$, $\dot{m}_{RA,ref}$ and $\dot{m}_{SA,ref}$ need to be determined for the objective function. As mentioned in Section 3.2.2, the return air temperature of $AHU9$ is a weighted average from room temperature in the office space of the SE1 building. Thus, the set point of each room temperature can be a reference for the state of return air temperature, that is,

$$T_{RA,ref} = \sum_{i=1}^{32} \rho_i T_{set,i}, \tag{3.20}$$

where $T_{set,i}$ is the set point of room temperature in each zone and ρ_i is the weight of each zone. Similarly, the reference of supply air reference can be expressed as the summation of the set point of discharge air flow rate in each zone,

$$\dot{m}_{SA,ref} = \sum_{i=1}^{32} \dot{m}_{set,i} \tag{3.21}$$

And the return air flow rate reference is proportional to the supply air reference,

$$\dot{m}_{RA,ref} = \alpha \dot{m}_{SA,ref} \tag{3.22}$$

The ratio α is calculated from the designed set point and the historic data from summer 2014. Since we use historic air flow rates as reference, the effect of fan powers can be neglected according to the affinity law.

After the parameter identification, now we can apply the gradient to the objective function. Take prediction horizon $p = 2$, control horizon $m = p - 1 = 1$ as an example:

$$\begin{bmatrix} \frac{\partial J^*}{\partial x_1(k+2|k)} \\ \frac{\partial J^*}{\partial x_2(k+2|k)} \\ \frac{\partial J^*}{\partial \Delta u_1(k|k)} \\ \frac{\partial J^*}{\partial \Delta u_2(k|k)} \\ \frac{\partial J^*}{\partial \Delta u_3(k|k)} \\ \frac{\partial J^*}{\partial \lambda(k+2)} \\ \frac{\partial J^*}{\partial \mu(k+2)} \end{bmatrix} = \begin{bmatrix} \frac{\partial J^*}{\partial T_{RA}(k+2|k)} \\ \frac{\partial J^*}{\partial \dot{m}_{RA}(k+2|k)} \\ \frac{\partial J^*}{\partial \Delta \beta(k|k)} \\ \frac{\partial J^*}{\partial \Delta T_{SA}(k|k)} \\ \frac{\partial J^*}{\partial \Delta \dot{m}_{OA}(k|k)} \\ \frac{\partial J^*}{\partial \lambda(k+2)} \\ \frac{\partial J^*}{\partial \mu(k+2)} \end{bmatrix} = \mathbf{0}, \tag{3.23}$$

where

$$\frac{\partial J^*}{\partial T_{RA}(k+2 \mid k)} = 2Q_1(T_{RA}(k+2 \mid k) - T_{RA,ref}(k+2)) + \lambda(k+2), \tag{3.24}$$

$$\frac{\partial J^*}{\partial \dot{m}_{RA}(k+2 \mid k)} = 2Q_2(\dot{m}_{RA}(k+2 \mid k) - \dot{m}_{RA,ref}(k+2)) + \mu(k+2), \tag{3.25}$$

$$\begin{aligned}\frac{\partial J^*}{\partial \Delta\beta(k \mid k)} &= c_p\dot{m}_{RA}(k+1 \mid k)(T_{RA}(k+1 \mid k) - T_{SA}(k) - \Delta T_{SA}(k \mid k)) \\ &+ 2Q_3\dot{m}_{RA}(k+1 \mid k)(\dot{m}_{RA}(k+1 \mid k)(\beta(k) + \Delta\beta(k \mid k)) \\ &+ (\dot{m}_{OA}(k) + \Delta\dot{m}_{OA}(k \mid k)) - \dot{m}_{SA,ref}(k+1)) \\ &+ 2R_1\Delta\beta(k \mid k) - b_{t,1}\lambda(k+2) - b_{f,1}\mu(k+2),\end{aligned} \tag{3.26}$$

$$\begin{aligned}\frac{\partial J^*}{\partial \Delta T_{SA}(k \mid k)} &= -c_p(\dot{m}_{OA}(k) + \Delta\dot{m}_{OA}(k \mid k) \\ &+ (\beta(k) + \Delta\beta(k \mid k))\dot{m}_{RA}(k+1 \mid k)) \\ &+ 2R_2\Delta T_{SA}(k \mid k) - b_{t,2}\lambda(k+2) - b_{f,2}\mu(k+2),\end{aligned} \tag{3.27}$$

$$\begin{aligned}\frac{\partial J^*}{\partial \Delta\dot{m}_{OA}(k \mid k)} &= c_p(T_{oa}(k+1) - (T_{SA}(k) + \Delta T_{SA}(k \mid k)) \\ &+ 2Q_3(\dot{m}_{OA}(k) + \Delta\dot{m}_{OA}(k \mid k) \\ &+ (\beta(k) + \Delta\beta(k \mid k))\dot{m}_{RA}(k+1 \mid k)) \\ &+ 2R_3\Delta\dot{m}_{OA}(k \mid k) - b_{t,3}\lambda(k+2) - b_{f,3}\mu(k+2),\end{aligned} \tag{3.28}$$

$$\begin{aligned}\frac{\partial J^*}{\partial \lambda(k+2)} &= T_{RA}(k+2 \mid k) - (a_t T_{RA}(k+1 \mid k) + b_{t,1}(\beta(k) + \Delta\beta(k \mid k)) \\ &+ b_{t,2}(T_{SA}(k) + \Delta T_{SA}(k \mid k)) + b_{t,3}(\dot{m}_{OA}(k) + \Delta\dot{m}_{OA}(k \mid k)) \\ &+ c_t T_{oa}(k+1)),\end{aligned} \tag{3.29}$$

$$\begin{aligned}\frac{\partial J^*}{\partial \mu(k+2)} &= \dot{m}_{RA}(k+2 \mid k) - (a_f\dot{m}_{RA}(k+1 \mid k) + b_{f,1}(\beta(k) + \Delta\beta(k \mid k)) \\ &+ b_{f,2}(T_{SA}(k) + \Delta T_{SA}(k \mid k)) + b_{f,3}(\dot{m}_{OA}(k) + \Delta\dot{m}_{OA}(k \mid k)) \\ &+ c_f T_{oa}(k+1)),\end{aligned} \tag{3.30}$$

Actually Equations (3.29) and (3.30) are the state equations that predict the value of the sates at the time interval $k+2$. They serve as the dynamical constraints

inside the optimization problem. If we put all the constants on the right-hand-side, the equations can be represented in the matrix form

$$\begin{bmatrix} \mathbf{Q} & \mathbf{0} & \mathbf{I}_2 \\ \mathbf{0} & \mathbf{R} & \mathbf{B}^T \\ \mathbf{I}_2 & \mathbf{B} & \mathbf{0} \end{bmatrix} \begin{bmatrix} T_{RA}(k+2 \mid k) \\ \dot{m}_{RA}(k+2 \mid k) \\ \Delta\beta(k \mid k) \\ \Delta T_{SA}(k \mid k) \\ \Delta\dot{m}_{OA}(k \mid k) \\ \lambda \\ \mu \end{bmatrix} = \mathbf{d}, \tag{3.31}$$

where

$$\mathbf{Q} = 2 \begin{bmatrix} Q_1 & 0 \\ 0 & Q_2 \end{bmatrix}, \tag{3.32}$$

$$\mathbf{R} = \begin{bmatrix} -2\delta\dot{m}_{RA}^2(k+1 \mid k) - 2R_1 & c_p\dot{m}_{RA}(k+1 \mid k) & -2Q_3\dot{m}_{RA}(k+1 \mid k) \\ -c_p\dot{m}_{RA}(k+1 \mid k) & -2R_2 & c_p \\ -2Q_3\dot{m}_{RA}(k+1 \mid k) & c_p & -2\delta - 2R_3 \end{bmatrix}, \tag{3.33}$$

$$\mathbf{B} = \begin{bmatrix} b_{t,1} & b_{t,2} & b_{t,3} \\ b_{f,1} & b_{f,2} & b_{f,3} \end{bmatrix}. \tag{3.34}$$

And the right-hand-side is a vector of constant, which is

$$\mathbf{d} = [d_1, d_2, d_3, d_4, d_5, d_6, d_7]^T, \tag{3.35}$$

where

$$d_1 = Q_1 T_{RA,ref}(k+2), \tag{3.36}$$

$$d_2 = Q_2 \dot{m}_{RA,ref}(k+2) \tag{3.37}$$

$$\begin{aligned} d_3 = {} & c_p\dot{m}_{RA}(k+1 \mid k) T_{RA}(k+1 \mid k) \\ & + 2Q_3\dot{m}_{RA}(k+1 \mid k)(\dot{m}_{OA}(k \mid k) + \beta(k \mid k)\dot{m}_{RA}(k+1 \mid k) \\ & - \dot{m}_{SA,ref}(k+1)), \end{aligned} \tag{3.38}$$

$$d_4 = -c_p(\dot{m}_{OA}(k \mid k) + \beta(k \mid k)\dot{m}_{RA}(k+1 \mid k)), \tag{3.39}$$

$$\begin{aligned} d_5 = {} & c_p(T_{oa}(k+1) - T_{SA}(k \mid k)) \\ & + 2Q_3(\dot{m}_{OA}(k \mid k) + \beta(k \mid k)\dot{m}_{RA}(k+1 \mid k) \\ & - \dot{m}_{SA,ref}(k+1)), \end{aligned} \tag{3.40}$$

$$\begin{aligned} d_6 = {} & a_t T_{RA}(k+1 \mid k) + b_{t,1}\beta(k \mid k) + b_{t,2} T_{SA}(k \mid k) + b_{t,3}\dot{m}_{OA}(k \mid k) \\ & + c_t T_{oa}(k+1), \end{aligned} \tag{3.41}$$

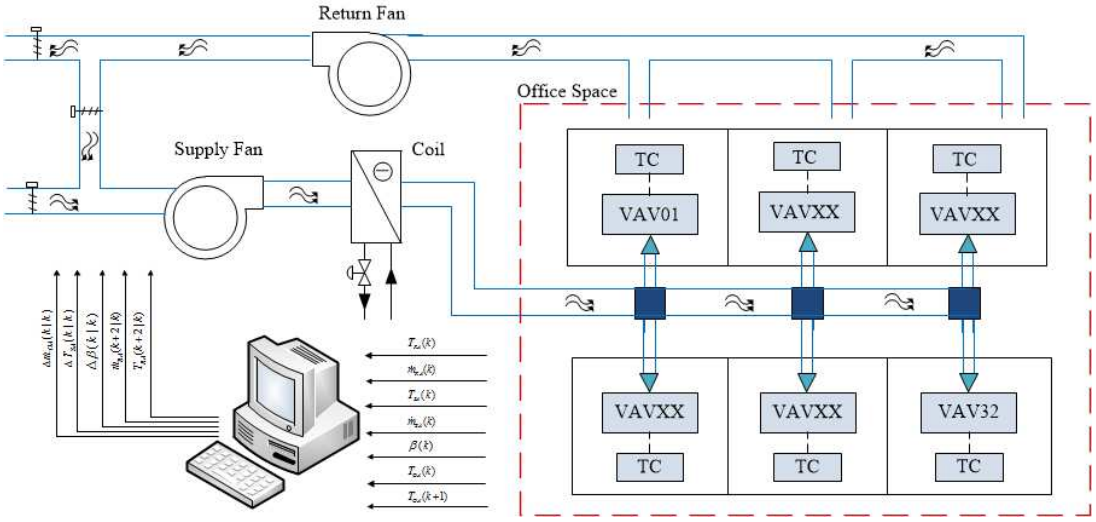

Figure 3.6: The MPC structure of the HVAC system of the SE1 building.

$$d_7 = a_f \dot{m}_{RA}(k+1 \mid k) + b_{f,1}\beta(k \mid k) + b_{f,2}T_{SA}(k \mid k) + b_{f,3}\dot{m}_{OA}(k \mid k) + c_f T_{oa}(k+1). \tag{3.42}$$

During one time interval, both control inputs $\beta(k)$, $T_{SA}(k)$ and $\dot{m}_{OA}(k)$, as well as the states $T_{RA}(k)$ and $\dot{m}_{RA}(k)$ at kth step. Furthermore, the states $T_{RA}(k+1 \mid k)$, and $\dot{m}_{RA}(k+1 \mid k)$ at next step can be computed according to the state equation (3.13). Therefore they can be considered as constants. In this problem, there are 7 unknowns and 7 equations. This system can be solved explicitly if there exists a unique solution.

It should be noted that this problem follows the form of "$\mathbf{Ax} = \mathbf{b}$" and the "$\mathbf{A}$" matrix here is even a symmetric matrix. This property makes this gradient based optimization problem easy to solve and implement in programming. For a symmetric indefinite matrix like this, LDL^T decomposition [88] can be used to solve the linear system.

The control formulation can be visualized as Figure 3.6. For every time interval, the data is read from sensors of the HVAC system in SE1 to the computer. The gradient based optimal control is computed and future states and control variables are computed. After that the future control variables are communicated from the online control system to the AHU. After that, the steps repeat in the next time span.

Chapter 4

NUMERICAL RESULTS

4.1 Mathematical Model Evaluation

4.1.1 Data Preprocessing

Measurements from thirty VAVs and AHU9 are available for the development of the ARMAX model. From May 1 to July 31, 2014, measurements of temperature T_{OA}, T_{MA}, T_{SA} and T_{RA}; air flow rates $\dot{m}_{OA}$, $\dot{m}_{RA}$, and $\dot{m}_{SA}$; damper positions D_{OA}, D_{RA} and D_{EA}; fan power W_{SF} and W_{RF} from AHU9, room temperature T_{rm} and its set point of $T_{rm,sp}$, the discharge air flow rate $\dot{m}_{dis}$ and its demand set point $\dot{m}_{dis,sp}$ from each affiliated VAV have been collected over 26 days with a sampling interval of fifteen minutes, resulting in $2,496$ samples. The BAS of the SE1 building applies a different operation strategy during the day from 7:30am to 1am, and during the night from 1am to 7:30am. During the day time, the HVAC system shows a diverse dynamics and more control efforts are imposed since the internal thermal load is higher. It's called occupied mode for WebCTRL®. The operation mode in the night is called unoccupied mode. Most of the occupants work during the day. The difference in occupancy between weekdays and weekends is insignificant. We divide the data by day and night with the same time partition and focus on the data that falls under occupied mode.

4.1.2 Data Smoothing

The measurements from HVAC systems have noise. In the SE1 building, the measurements are read from sensors and then linked to the BAS. Noise is also part of the sensor readings and not good for the parameter identification of linear regression. The sensor location, and lack of routine maintenance affect the accuracy of the measurements. Sensor noise in HVAC systems are regarded as white random noise [89]. However, the estimation of bias is sensitive to the measurements scale [90]. The real bias is not easy to find. Thus, a smoothing method, the Savitzky-Golay filter [91], is used for denoising in flow rate measurements of the SE1 building Typical filters, like the plain FIR filter, might remove useful high-frequency signals in measurements [92]. Savitzky-Golay filter, also known as a polynomial smoothing, or least-squares smoothing filter can preserve better high-frequency information. The polynomial fitting is equivalent to discrete convolution across a moving window

on the time domain. It is a low-pass filter that maintains the shape and height of waveform peaks [93]. These properties are beneficial to the HVAC system's measurements noise reduction. For flow rate measurements, the peaks represent the high demand of the cooling load of the building. Also, the HVAC system's dynamic is relatively slow compared to the sampling interval and the measurements are periodic in shape day by day. The preservation of the peak and shapes can help us save the useful content for modeling while reducing noise.

Consider a measurement $\mathbf{x}$ in a group with M sampling numbers. The data $x(n)$ at the center of a moving window is set as $n = 0$. It is the target filter data. All the points of $x(n)$ in this zone can be approximated with a polynomial as

$$p(n) = \sum_{k=0}^{N} a_k n^k, \tag{4.1}$$

where k is the order of each term and N is the highest order of the polynomial. The smoothed output value $y(0)$ is obtained by evaluating $p(n)$ at $n = 0$, which is

$$y(0) = p(0) = a_0. \tag{4.2}$$

That means, the value of smoothed data is equal to the 0th order polynomial value. To find a_0, the optimal coefficients need to be calculated. The optimal coefficients can be found by minimizing the mean squared error (MSE) of Equation (4.1). for the points in the zone,

$$\begin{aligned} \varepsilon_N &= \sum_{n=-\frac{M-1}{2}}^{\frac{M-1}{2}} (p(n) - x(n))^2 \\ &= \sum_{n=-\frac{M-1}{2}}^{\frac{M-1}{2}} (\sum_{k=0}^{N} a_k n^k - x(n))^2. \end{aligned} \tag{4.3}$$

Thus, differentiation is applied to ε_N in Equation (4.3) with respect to each sample of the N+1 unknown coefficients and setting the corresponding derivatives equal to 0. Thus, for $i = 0, 1, \ldots, n$,

$$\frac{\partial \varepsilon_N}{\partial a_i} = \sum_{n=-\frac{M-1}{2}}^{\frac{M-1}{2}} 2n^i (\sum_{k=0}^{N} a_k n^k - x(n)),$$

which can be rewritten as

$$\sum_{k=0}^{N} (\sum_{n=-\frac{M-1}{2}}^{\frac{M-1}{2}} n^{k+i}) a_k = \sum_{n=-\frac{M-1}{2}}^{\frac{M-1}{2}} n^i x(n). \tag{4.4}$$

To solve Equation (4.4), a M by $N+1$ matrix $\mathbf{A}$ can be defined as $\mathbf{A} = \{n^i\}$ for $i = 0, 1, \ldots, n$, and a $N+1$ by $N+1$ symmetric matrix $\mathbf{B} = \mathbf{A}^T\mathbf{A}$. Thus Equation 4.4 can be represented as

$$\mathbf{Ba} = \mathbf{A}^T\mathbf{Aa} = \mathbf{A}^T\mathbf{x}, \tag{4.5}$$

where $\mathbf{a} = [a_0, a_1, \ldots, a_N]^T$, and $\mathbf{x} = [x(-\frac{M-1}{2}), \ldots, x(-1), x(0), x(1), \ldots, x(\frac{M-1}{2})]$. Therefore, the solution of the polynomial coefficient can be written as

$$\mathbf{a} = (\mathbf{A}^T\mathbf{A})^{-1}\mathbf{A}^T\mathbf{x} = \mathbf{Hx}. \tag{4.6}$$

Recall that from the output of Equation (4.2) only a_0 is need for approximation. Thus, only the first row of H matrix is needed to compute a_0. Using $h_{0,m}$ to denote the elements of the first row of the H matrix, the smoothed data can be represented as

$$y(0) = a_0 = \sum_{m=-\frac{M-1}{2}}^{\frac{M-1}{2}} h_{0,m}x(m), \tag{4.7}$$

where it is obvious that all the data in the zone is used to smooth the value target point.

In the design of Savitzky-Golay filter, the selection of M and N affects the result of the smoothed data. A too large N close to M can lead to a badly conditioned H matrix. A huge window size of M can result in excessive information from the past and future. For our problem, M is chosen as 5 since it only contains the content of points from $n-2$ to $n+2$ for the nth measurement. This is consistent with the length of the prediction horizon of our approach. The highest polynomial order N is set to 3. Therefore, the smoothed data at the nth step can be represented as

$$y(n) = \frac{1}{35}(-3x(n-2) + 12x(n-1) + 17x(n) + 12x(n+1) - 3x(n+2)), \tag{4.8}$$

where the coefficients are calculated from the first row of the 4 by 5 H matrix.

Figure 4.1 shows the smoothing effect of the Savitzky-Golay filter on the return air flow rate of AHU9 in the SE1 building. The data is sampled during 26 days in May, 2014. The high-frequency oscillation of the original data is reduced. Meanwhile, the shape and peaks of the data are preserved. The average value of the smoothed data remains the same as the raw data, $7,362$ cubic meter per minute (cfm). This proves it is feasible to obtain smoothed data for modeling and control. The comparison of the model validation with both the raw data and the smoothed data will be provided in Section 4.1.4.

However, the Savitzky-Golay filter cannot be implemented to real time since it needs future measurements. A low-pass filter, such as the Butterworth filter [94] is

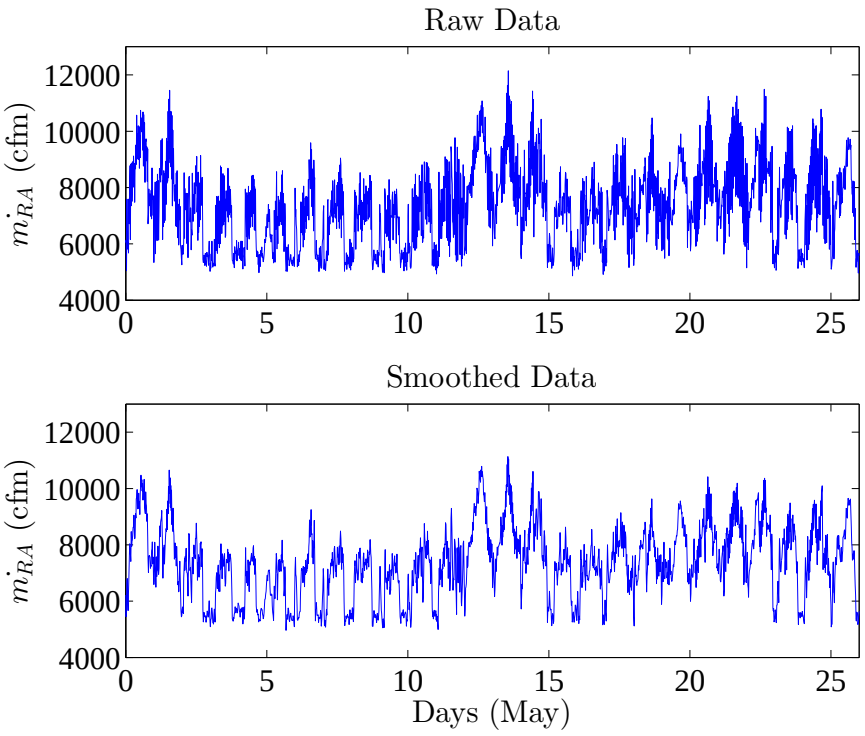

Figure 4.1: Comparison of the raw data (upper subplot) with the smoothed data by the Savitzky-Golay filter (lower subplot) in May, 2014.

used in real time data smoothing here. This filter has a property of a maximally flat magnitude in the passband [95]. The design of Butterworth filter can be specified by two parameters, the order of filter n and the cutoff frequency ω_c [96].

The Butterworth filter is widely used for data smoothing in different fields, such as handwriting movement [97], inertia navigation system [98] and biomechanics [99]. It has a sufficient accuracy with a low programming effort. However, in digital implementation, the phase delay introduced by this filter has to be considered. The dynamics of the HVAC system is slow. A small time delay is acceptable. An order of filter $n = 2$ and a normalized cutoff frequency $\omega_c = 0.5$ are selected. The resulting digital filter brings one step time delay. It should be noted that the second order is also consistent to the prediction horizon as well as the order of the Savitzky-Golay filter considered earlier.

The transfer function of a second order Butterworth filter can be written as

$$H(s) = \frac{1}{(\frac{s}{\omega_c})^2 + 1.4142\frac{s}{\omega_c} + 1}. \tag{4.9}$$

The bilinear transform is used to convert it to digital time domain

$$s \approx \frac{2}{T}\frac{1 - z^{-1}}{1 + z^{-1}}, \tag{4.10}$$

where T is the sample period. We define $K \triangleq \frac{2}{T}$. This results in the digital Butterworth filter form as

$$\begin{aligned} H_d(z) &= \frac{1 + 2z^{-1} + z^{-2}}{((\frac{K}{\omega_c})^2 + 1.4142\frac{K}{\omega_c} + 1) + (2 - 2(\frac{K}{\omega_c})^2)z^{-1} + ((\frac{K}{\omega_c})^2 - 1.4142\frac{K}{\omega_c} + 1)z^{-2}} \\ &\approx \frac{0.2929 + 0.5858z^{-1} + 0.2929z^{-2}}{1 + 0.1716z^{-2}}. \end{aligned} \tag{4.11}$$

The difference equation of the smoothed data $y(n)$ at the nth step from raw measurement $x(n)$ can be represented as

$$y(n) = 0.2929x(n) + 0.5858x(n-1) + 0.2929x(n-2) - 0.1716y(n-2). \tag{4.12}$$

The example of the Butterworth data smoothing is shown in Figure 4.2. The high frequency noise has been reduced, meanwhile the phase delay is reasonably small.

4.1.3 Model Validation

We identify the collection of coefficients $\mathbf{a}$, $\mathbf{b}_1$, $\mathbf{b}_2$,$\mathbf{b}_3$ and c with the method of least squares by using Equation (3.13). The least square solution of those three parameters is obtained by using the backslash operator in MATLAB [100]. The

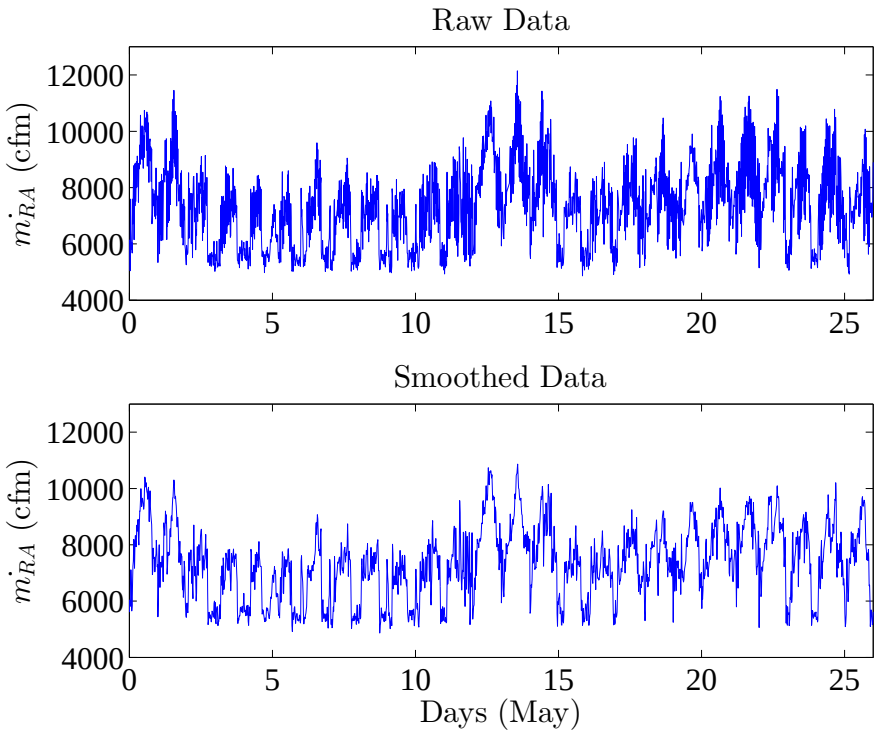

Figure 4.2: Comparison of the raw data (upper subplot) with the smoothed data by the Butterworth filter (lower subplot) in May, 2014.

method to numerically determine the optimal number of samples for parameter identification has been discussed in the previous work of our group [50, 53].

To validate the model, we first select a metric for evaluating the accuracy of prediction. In literature regarding data analysis of time series [101–105], it is common to use the mean absolute error (MAE), MSE, the root mean squared error ($RMSE$), coefficient of determination (r^2) and maximum absolute error ($MaxAE$). These are defined as

$$MAE = \frac{1}{m}\sum_{i=1}^{m} |X_i - X_i^*|, \tag{4.13}$$

$$MSE = \frac{1}{m}\sum_{i=1}^{m} (X_i - X_i^*)^2, \tag{4.14}$$

$$RMSE = [\frac{1}{m}\sum_{i=1}^{m} (X_i - X_i^*)^2]^{1/2}, \tag{4.15}$$

$$r^2 = \frac{(m\sum X_i X_i^* - (\sum X_i)(\sum X_i^*))^2}{(m(\sum X_i^2) - (\sum X_i)^2)(m(\sum X_i^{*2}) - (\sum X_i^*)^2)}, \tag{4.16}$$

$$MaxAE = \max_i |X_i - X_i^*|, \tag{4.17}$$

where X_i, and X_i^* are the estimated values and measurements of a particular attribute in the time domain, respectively, and m is the total number of measurements.

Figure 4.3 presents a three-day return air temperature prediction of $AHU9$ in July. The data from July 1 to July 6 is used for linear regression to determine the coefficients, and the model is implemented into July 7 to July 9 for prediction. The prediction horizon is set to be 2. It is observed that the prediction matches well with the measured T_{ra}. The MSE is 0.0059. The prediction captures the abrupt fluctuations under the occupied mode.

Modeling and prediction are conducted to data from 62 days in May, June and July during summer 2014. For May and June, the same number of prediction days are considered; 7 is used as a relatively long time prediction and the numbers of training days are 19 and 22 respectively. A shorter training length of 6 days is applied to data from July, followed by a three-day prediction. The results of the return air model are shown in Table 4.1. It can be seen that the error doesn't change with different months during the summer time. Additionally, the order of magnitude of the error remains small for both short and long term modeling and prediction.

Since our model is flexible to variable prediction lengths, we can investigate the relationship between the prediction error and prediction horizon. Table 4.2 shows the return air model validation results for $AHU9$ of the SE1 building. From the

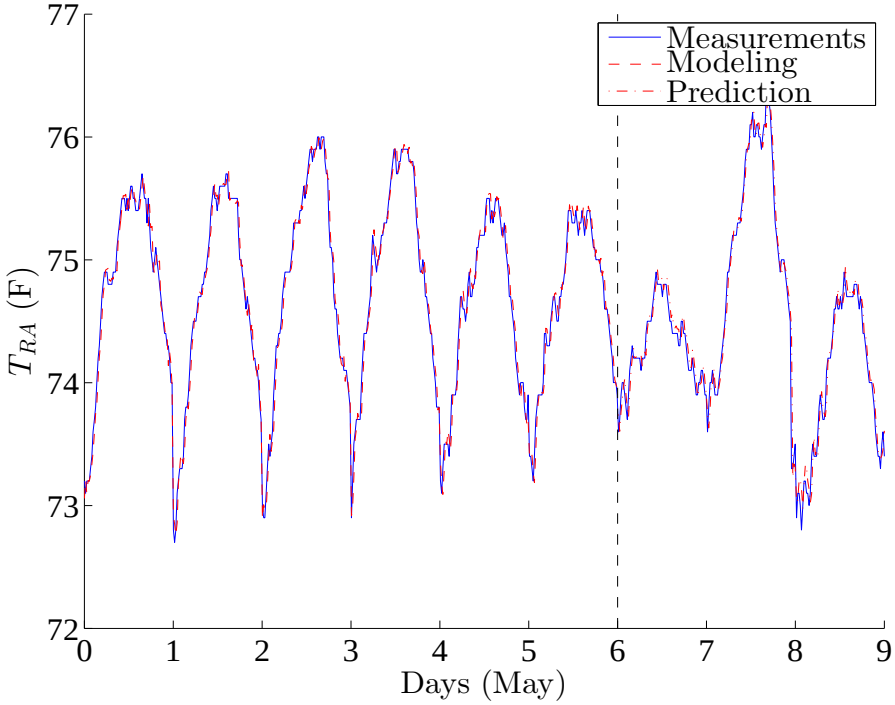

Figure 4.3: The three-day return air temperature prediction of $AHU9$ with the FIR model. The prediction tracks the measured temperature on the slope well and captures the oscillation at peaks.

Table 4.1: The errors of the return air temperature prediction of multiple months.

Month	Training Days	Prediction Days	MAE	MSE	$RMSE$	r^2	$MaxAE$
May	19	7	0.0579	0.0059	0.0769	0.9743	0.3631
June	22	7	0.0592	0.0056	0.0750	0.9647	0.2333
July	6	3	0.0515	0.0055	0.0741	0.9724	0.6395

table, we can find that the prediction errors drop slightly and gradually the highest order the model increases. For further consideration and comparison, Figure 4.4 gives a plot of coefficient of determination to different lengths of prediction horizons respect to models of the return air temperature and return air flow. Compare with the return air flow rate model, the return air temperature is more accurate to the measurements. In a recent work [48], ARMAX type models have been claimed to be very effective to model room temperature with relatively small prediction errors in the summer. According to Section 3.2.2, the return air of $AHU9$ can be considered as a weighted average of office zone temperatures in the SE1 building. Therefore, the accuracy of this model is also valid. From the figure we can find that the coefficient of determination of the return air model remains stable when the length of the prediction horizon increases. For the flow rate model, because of high-frequency noise and unacceptable fluctuation during each trend cycle, the accuracy is limited for an ARMAX model. The filter used here for air flow rate data smoothing is the Butterworth filter.

However, when a higher order is involved in the model, the coefficient of determination rises. From Figure 4.4, we can also find that the slope of increasing of r^2 becomes flat with a longer prediction horizon. In addition, in ARMAX and MPC, a huge prediction horizon will significantly burden the computation load. It cannot be neglected that the coefficient of determination of the return air model slightly drops when the prediction length becomes larger. For the modeling of temperature, it is reasonable to sample during a shorter moving window. This is because the return air temperature here has peaks during the day time under occupied mode. If the data of the current time interval is located in transition area, a larger order model involved too many points before will affect the linear regression result. Therefore, there is a trade-off between the prediction length, the accuracy of both models and the complexity of the computation. In the simulation, a prediction length $p = 2$ is used in our control algorithm.

It should be noted that the model (3.5) can be regarded as a discrete form of a first order ordinary differential equation (ODE) when it $p = 1$ since the coefficient of $T_{RA}(n - i)$ is 0.9722, nearly 1. This value follows the form a forward difference equation.

4.1.4 Comparison with Raw Data Model

In Section 4.1.2 data smoothing by the Savitzky-Golay filter and the Butterworth filter is implemented into the raw data of return air flow rate measurements to make it more feasible for linear regression results of the ARMAX model. The comparison between the raw data, and smoothed data by the Savitzky-Golay filter and the Butterworth filter has been provided in Figure 4.1 and 4.2 respectively. Now

Table 4.2: The return air temperature prediction error over different prediction horizons.

Prediction Horizon	MAE	MSE	$RMSE$	r^2	$MaxAE$
1	0.0579	0.0059	0.0769	0.9743	0.3631
2	0.0543	0.0054	0.0733	0.9769	0.3630
3	0.0553	0.0052	0.0720	0.9777	0.3604
4	0.0556	0.0052	0.0720	0.9776	0.3541

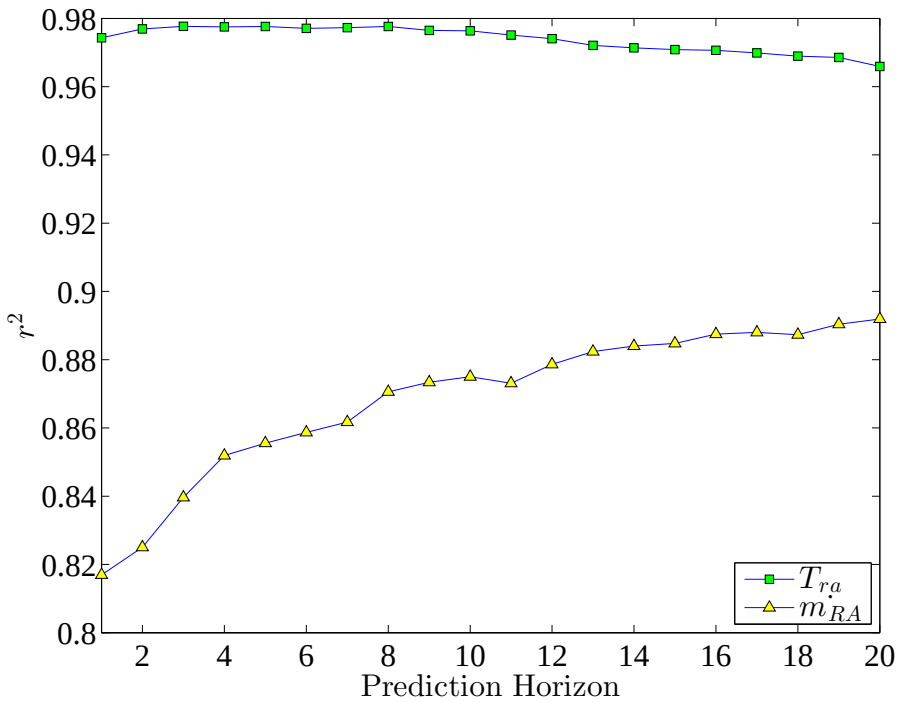

Figure 4.4: The coefficient of determination vs. the length of the prediction horizon during the summer.

Table 4.3: The return air flow rate modeling error with respect to raw data and smoothed data.

Data Type	MAE	MSE	$RMSE$	r^2	$MaxAE$
Raw Data	0.3371	0.1756	0.4191	0.6195	1.5902
Savitzky-Golay filter	0.1879	0.0553	0.2352	0.8452	0.8424
Butterworth filter	0.1710	0.0513	0.2264	0.8516	0.9220

we can study the difference from the model side. The same ARMAX modeling is applied to both the raw data and smoothed data, and the model validation result from May is shown in Table 4.1.4. Significant improvement can be observed from the modeling error after data smoothing. The result shows that the smoothed data are easier to work with using the ARMAX model. In addition, the modeling accuracy of smoothed data by the second order Butterworth filter with half normalized cutoff frequency is better than the seconder order Savitzky-Golay filter. It reduces more high-frequency oscillations. The plots of modeling with respect to these three types of data are also provided in Figure 4.5. It should be noted that the modeling to smooth data has better performance on fluctuation pattern and adds consistency to the slopes of the data shape.

In summary, the return air flow rate model with smoothed data and the return air temperature model are feasible to serve as the plant model for control design in this problem.

4.2 Control Simulation Results

The performance of the original local PID control and Lagrangian Multiplier based MPC control algorithm are compared through simulations. Simulations are conducted using MATLAB. The data is from May, June and July, 2014, consistent with that in our numerical modeling. The control strategies are applied to the office zone of the SE1 building, from 7:30am to 1am. All the figures in this section are generated with smoothed data by the second order Butterworth filter.

The results are evaluated from different angles. We both observe the results with different time spans. A daily energy track can be found in Figure 4.6 during 8am to 12am from July 1st, 2014. A peak of both energy consumption trends can be found between 4pm to 6pm can be found. This is actually the outside temperature peak hours in Merced as well. When outside air is hot, it takes more power from $AHU9$ to cool the mixing air down. This proves the feasibility of our energy flow model and the peak cost reduction can also be found from this figure.

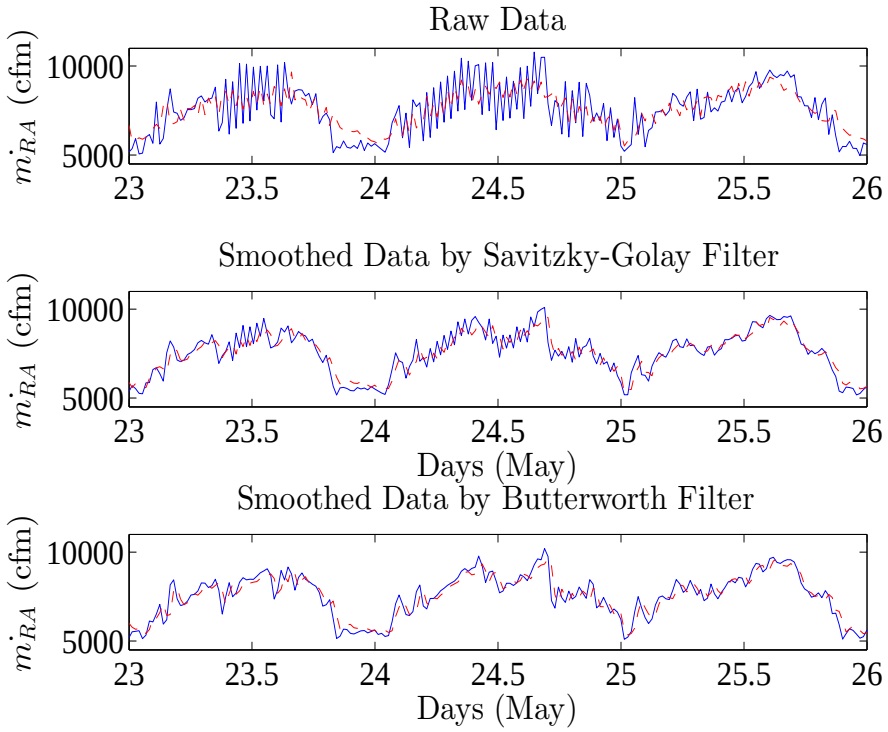

Figure 4.5: Comparison of three-days modeling trends in May with the raw data and smoothed data by two different low-pass filter. A better curve fitting can be observed from the smoothed data by Butterworth filter.

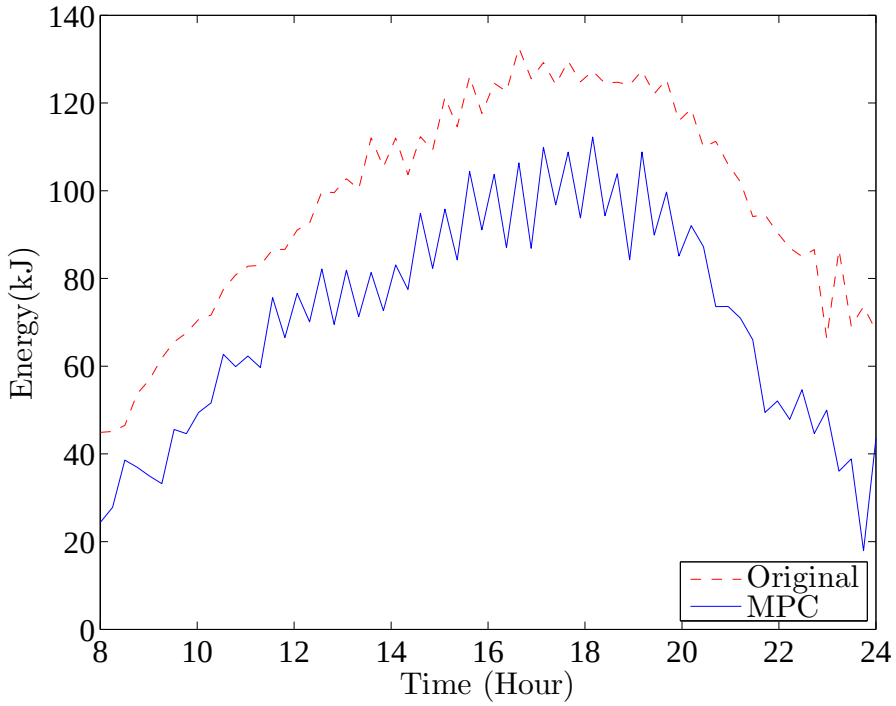

Figure 4.6: The energy flow of $AHU9$ by MPC and original control strategies under occupied mode during July 1st, 2014. The energy savings is obvious while the optimized energy flow has more oscillation due to a wider usage of dampers.

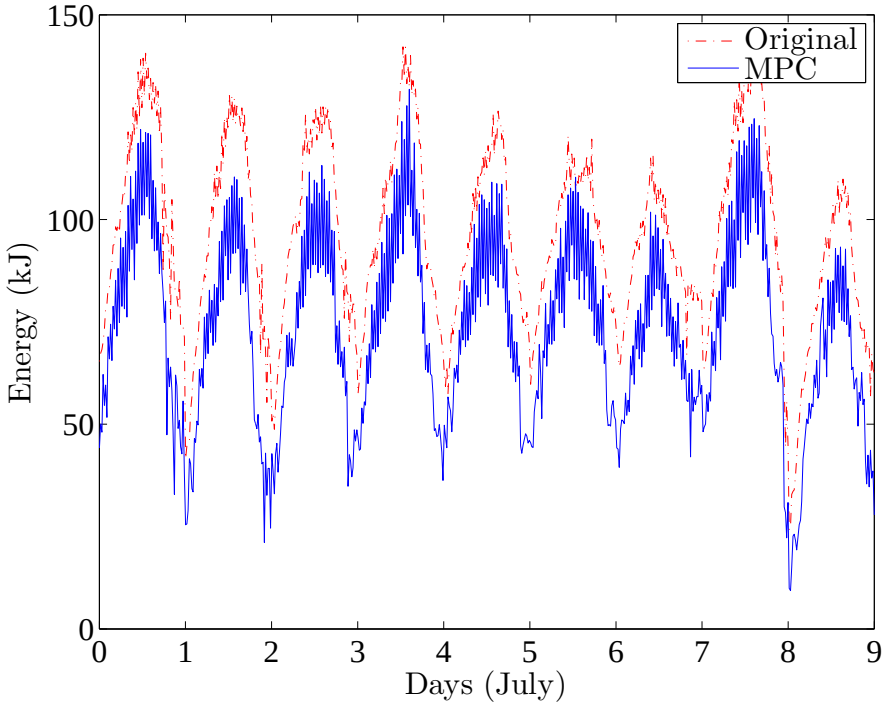

Figure 4.7: Energy consumption trends of $AHU9$ by MPC and original control strategies under occupied mode during the first 9 days in July, 2014. The average energy saving percentage is 25.7%.

4.7 shows the comparison of energy consumption of $AHU9$ with MPC for ten days in July. An obvious energy saving both at peaks and in total can be observed. Similar results can be also found from May and June, 2014. Compared to the energy flow of the existing control strategy, that from MPC has more oscillation since a wider usage of dampers. The time interval for our control approach is 15 minutes, that is enough for dampers to adjust to the new positions. In the objective function 3.15, the tracking error to references of room temperature set points, supply air flow rate and return air flow rate is also an evaluation of the simulation results.

To compare the control variables including the return air ratio β, Figure 4.8 is provided with hard bounds on both sides for a monthly evaluation. From the sub-plot of β, a larger range can be found, which increases the possibilities of a new combination of the outside air flow and the recirculation air flow even with the same supply air flow rate demand. As for supply air temperature T_{SA}, since the outside air in Merced is very dry, a higher supply air temperature set point can be used here to reduce the mechanical cooling load of water coil in $AHU9$. The average supply

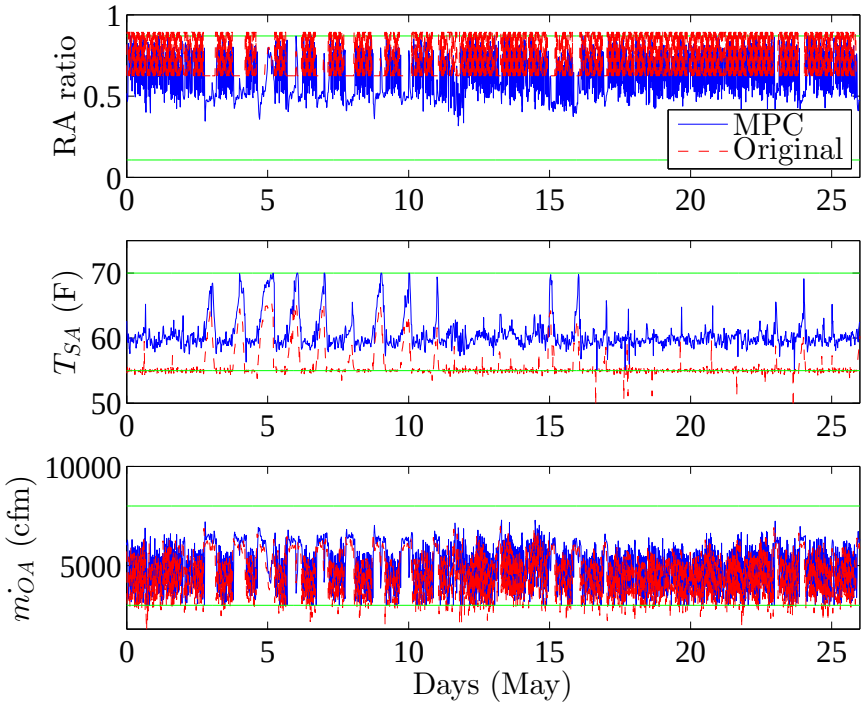

Figure 4.8: The control variables comparison between MPC and existing control in 26 days from May, 2014. A wider range of damper position, higher set point of supply air temperature and outside air flow rate can be observed.

air temperature set point before in 26 days of May is 55.68 F and that of MPC is 60.57 F. In addition, the third control variable, the outside air flow rate $\dot{m}_{OA}$, is slightly larger than that of original control strategy. As far as we know that under the occupied mode the average outside air temperature is already higher than that of return air during May. Absorbing more outside air may draw the potential to add the cooling load of the AHU. However, with a right combination with an optimal return air ratio β, and an optimal supply air temperature T_{SA}, an energy saving is achieved while higher outside air flow rate applied. It's good to have more outside air since the thermal comfort for office building requires enough fresh air.

To further investigate the air enconomizer behavior under two control strategies, the distribution and constitution of supply air flow rate is taken into account. The supply air flow includes the outside air flow and the recirculation air flow from the return air. From Figure 4.9 similarity in structure can be found under two

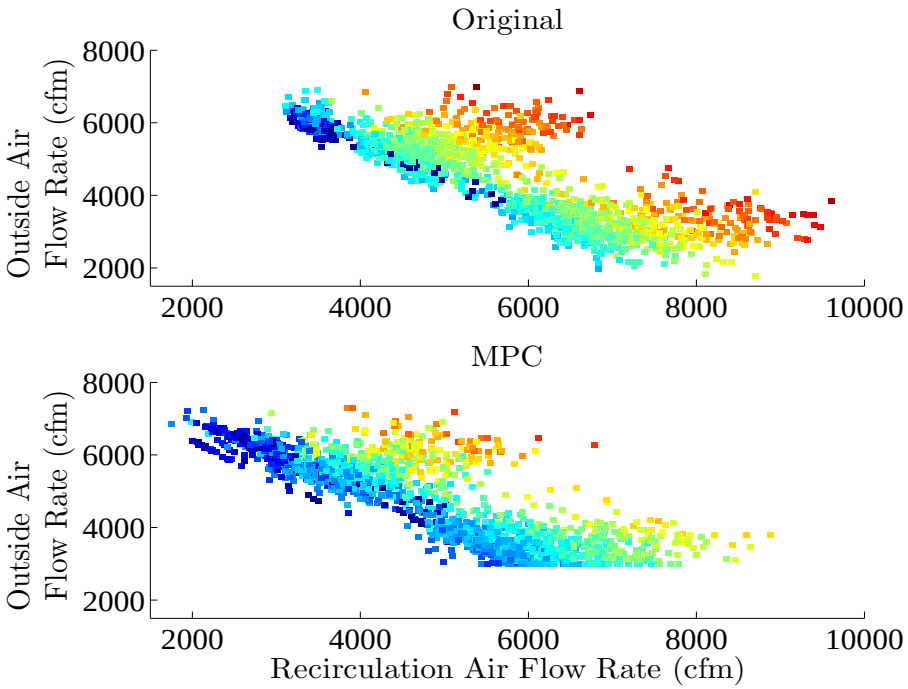

Figure 4.9: The distribution of the outside air flow rate and the recirculation air flow rate under the two control strategies follow the same structure.

control strategies. The color represents the value of the normalized energy and optimized energy consumption. The normalized values are obtained by dividing the absolute values of energy and optimized energy consumption by the maximum energy consumption under the existing control laws. Both if the results follow the similar structure, and it costs more when the summation of the outside air flow and the recirculation air flow becomes larger. Compared to the upper scatter, the lower figure shows a lower average and a strict bound for minimum outside air flow rate. It should be noted that the lowest energy cost on the northwest of both figures shows the case at the beginning and end of each occupied mode cycle. During those hours, the outside air temperature is relatively low so that the AHU absorbs a lot of outside air flow and the energy consumption is efficient.

The simulation results tell us that the outside air temperature is a dominant component in this problem. To further prove that, the relationship between outside air temperature and energy reduction is evaluated from two kinds of analysis, the daily analysis, and the hourly analysis. The correlation between daily average outside air temperature and the daily energy saving potential from the proposed

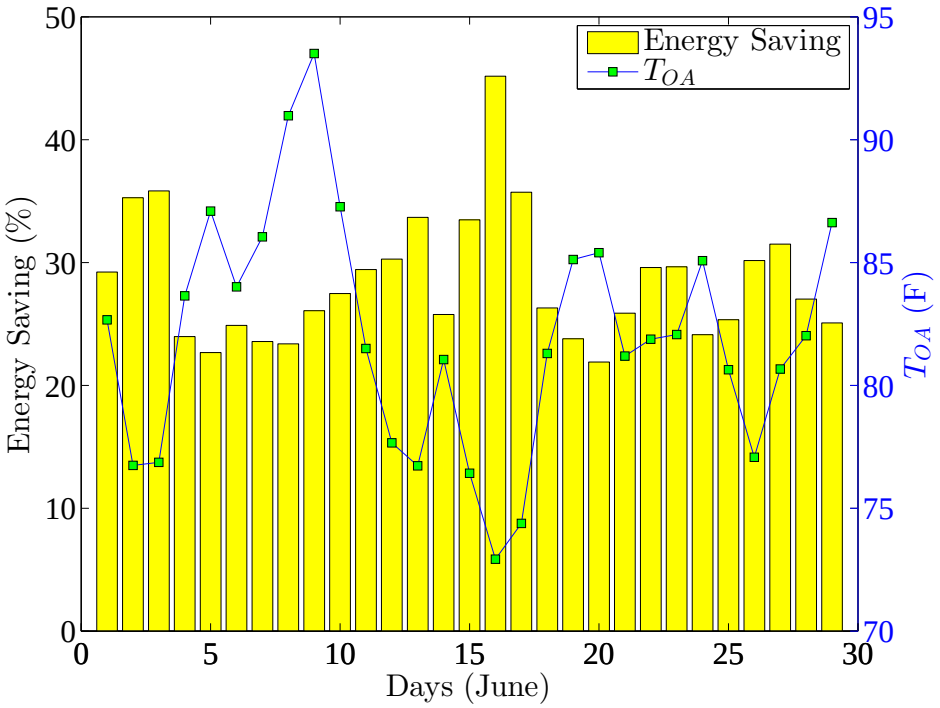

Figure 4.10: A negative correlation between outside air temperature and energy saving percentage in 20 days from June, 2014.

approach is shown in Figure 4.10. The dates with lower average outside air temperature have a better performance in energy saving. The correlation coefficient is 0.59. Note that the percentage cannot completely represent the actual saving. If the original energy cost is huge, even the energy saving percentage is small it is also huge beneficial to apply the proposed control algorithm.

Secondly, the hourly analysis is applied from different aspects. Figure 4.11 shows the average trends of the supply air and the outside air temperatures under occupied mode during 64 days of 2014 summer. The supply air temperature's change is related to that of the outside air temperature and thermal demands from occupants. During the peak hours of the outside air temperature, from 12pm to 8pm, the supply air remains 55 F for the entire time span. Thus, the difference between these two temperature reaches a maximum value at 5pm. During these hours, the HVAC system of the SE1 building needs to be fully operated to serve occupants enough cooling load although the outside air temperature is high.

To further analyze the operation of $AHU9$ during the daytime, the supply flow rate is also considered as a reference. The supply flow rate can be divided

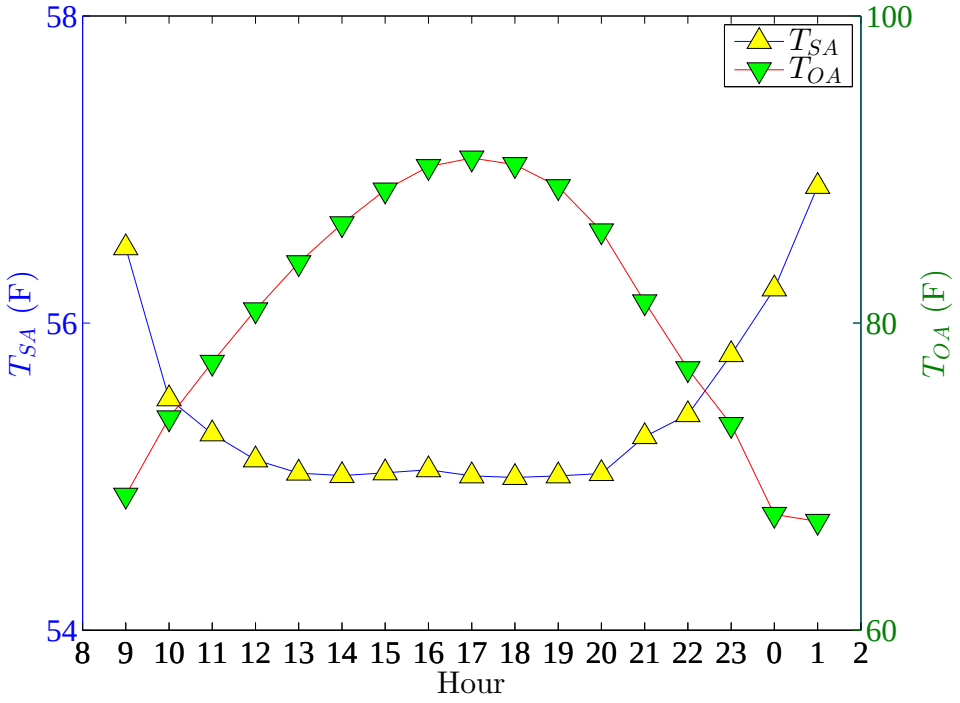

Figure 4.11: The average supply air and outside air temperatures under occupied mode from 64 days in 2014 summer.

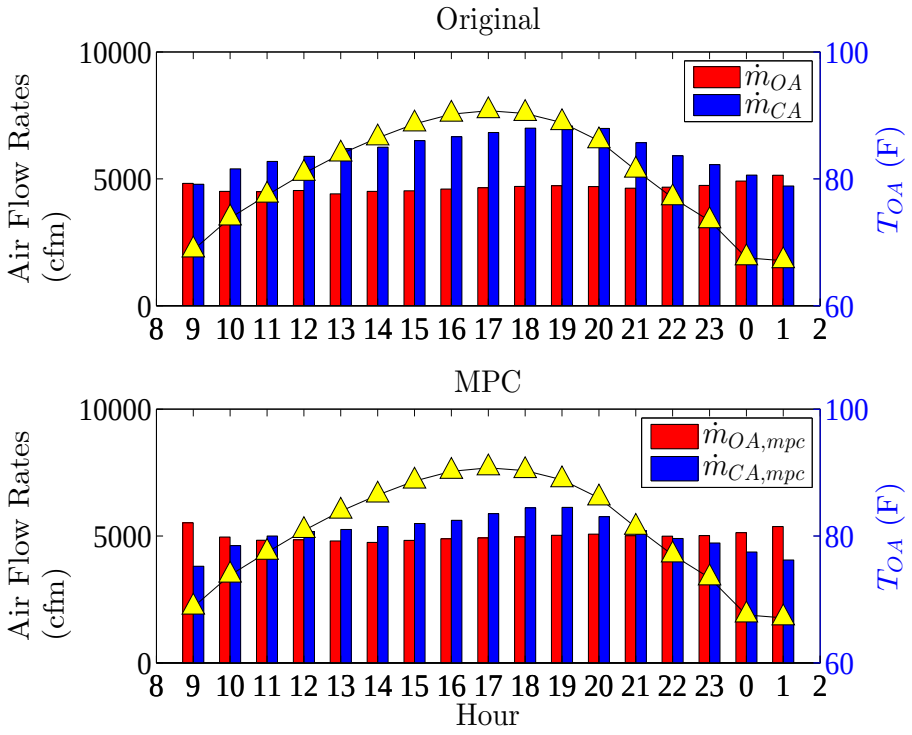

Figure 4.12: The comparison of the supply flow rate with the original and MPC control strategies.

into two parts, the outside air flow rate, and the recirculation air (CA) flow rate. Therefore, we compare the value of these two under both the original and MPC control strategies. Figure 4.12 shows that they also keep the same structure. During the peak hours of the outside air temperature, the value of supply air flow rate reaches its maximum. However, in the original control, the usage of outside air flow is limited during non-peak hours. For the time interval of the morning and the night, the outside air temperature is relatively low, and the demand of occupants is not as intensive as working hours. Therefore, more outside air flow and higher supply air temperature can be utilized to reduce the energy consumption. Under MPC control strategy, the values of the outside air flow rate are obviously greater than the original control before 12pm and after 20pm.

The hourly analysis of predictive energy savings percentage is also provided in Figure 4.13. For every hour, the actual energy reduction is nearly the same. Because the amount of energy consumption is different during different time interval, the predictive energy savings are relatively low during the peak hours and reach high level in the morning and night. The trend of energy saving potential is opposite to

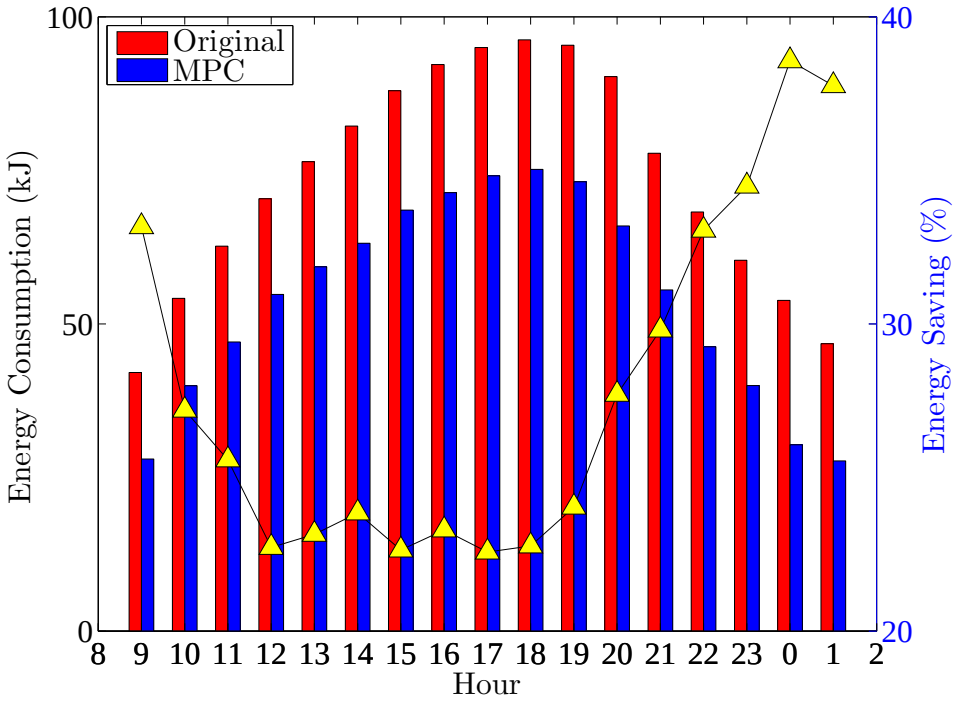

Figure 4.13: The absolute predictive energy savings remains the same under the occupied mode. Meanwhile, the energy savings potential percentage has the opposite trend to the outside air temperature.

the outside air temperature and working hour schedule.

To conclude, the MPC strategy is effective on energy efficiency of the AHU. The energy saving is achieved during every time span under occupied mode, however, the predictive energy reduction during the peak hour of the outside air temperature.

Except the energy savings, the control results should also be evaluated from the tracking error to the references. Figure 4.14 shows take the trends of the optimized return air temperature, the supply air flow rate, and the return air flow rate of $AHU9$ tracks the set points closely. To further prove that, the tracking error is calculated as MAE in Table 4.4. The tracking to the set point of the weighted average of room temperatures and supply air flow rate shows the cooling demand of the occupancy in building zones will be covered as the original control. In addition, the same return air flow rate ensure that the ventilation level and the building static pressure will not change due to the difference of the air flow exchange by applying a different control strategy.

Table 4.4: The tracking MAE of MPC control states to the reference values.

States	T_{RA}	$\dot{m}_{SA}$	$\dot{m}_{RA}$
MAE	0.00012	0.0592	0.0228

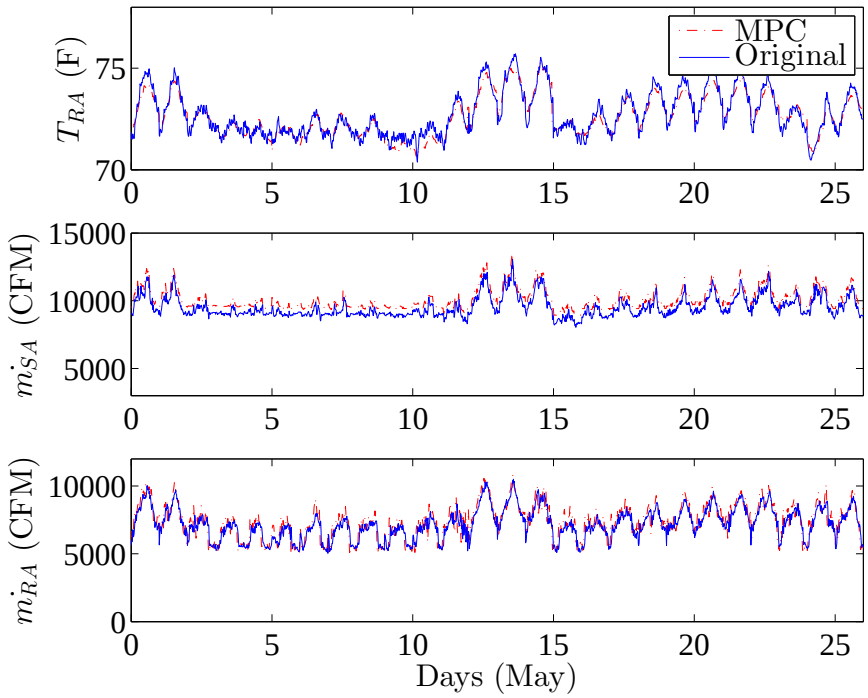

Figure 4.14: The optimized return air temperature, the supply air flow rate, and the return air flow rate track closely to the reference values.

Chapter 5

SUMMARY AND FUTURE WORK

5.1 Concluding Remarks

To leverage the untapped capabilities of modern building automation and control systems, we have developed a system-level dynamical model and MPC control design of HVAC systems. Works in this thesis focus on two functionalities, i.e., modeling and control. As for modeling, we have used a return air dynamical model to link the current temperature and flow rate states of the building and the control variables, that is accurate for prediction and friendly to control implementation. With regard to control, based on the model we built serving as a plant, a MPC algorithm is applied to the HVAC energy management system. This MPC strategy utilizes different levels of HVAC units in buildings. The control results show a significant energy saving meanwhile keep the same level of building cooling load, thermal comfort and static pressure. This algorithm can be applied on system-wide scales to optimize overall system performance and help achieve the goal of zero energy consumption.

5.1.1 Model

We have developed a FIR-based return air model from the AHU return air dynamics for both temperature and air flow rate. The proposed model has prediction and control horizon flexibility and much few variables compared to a fully numerical model. Trained with the data over a short and long time frame, the proposed model is capable of predicting the return air temperature with a high accuracy. For example, the AHU return air temperature model trained with the data from 2014 summer can predict the return air temperature over one week with mean squared errors less than 0.006 and coefficients of determination above 0.97 on average. We have also shown the relationship between prediction steps and the accuracy of the model. An optimal prediction horizon provides a trade-off between model accuracy and computation load. With the right choice of prediction horizon, the dynamical model further improves its prediction performance, and could be a basis for MPC control design of HVAC systems.

Otherwise, we implement Savitzky-Golay filter during data pre-processing for data smoothing. Measurements of air flow rate inside HVAC systems is vulnerable

to sensor noise and resistant to model parameter identification. Savitzky-Golay filter takes a moving average of the measurements and serves as a low-pass filter. After smoothing, the curve fitting performance becomes better and could be used as a plant of an MPC controller of HVAC systems.

It should be noted that this model could also be used to predict other parameters of interest in HVAC simulations, e.g., the relative humidity and parts per million (ppm) of CO_2. We are trying to corporate this model with the relative humidity sensors and CO_2 sensors of other latest buildings on UC Merced campus.

5.1.2 Control

We have established a system-level MPC control strategy for building HVAC systems. Energy description of the AHU and the gradient-based optimization and the cross-level constraints and objectives are three key elements of the method. The energy flow model provides the possibilities of variable distribution of outside air and recirculation air. This energy feature helps energy saving of the HVAC system and cover the thermal demand of the building, as well as preserve the same static pressure and ventilation level. The control strategy uses damper positions, supply air temperature and outside air flow rate as control variables. They are explicitly implemented into both the models and objective functions. The strategy provides physical-based inherent connection between components in AHU, and considers cross-level constraints in the whole HVAC system of SE1 building. For the optimization procedure, the gradient follows a fine structure due to the types of objective functions and the involvement of Lagrangian Multiplier. It might be an indefinite symmetric matrix, thus this linear system can be solved efficiently by some factorization method such. The optimal results show an energy saving average percentage over 27.8% and track the supply air flow rate and set point of room temperatures in the building pretty well. The thermal load, supply air flow rate set points are calculated from thirty-two VAVs, that ensures the internal cooling demand, the static pressure, and the ventilation level of the building.

This control strategy is implemented into the WebCTRL®of the SE1 building and can be easily incorporated with other BAS as well since the explicit formulation.

5.2 Future Work

5.2.1 MPC of HVAC systems with Humidity and CO_2 Control

Due to the scarcity of humidity sensors in SE1 building, the humidity control cannot be considered in our approach. However, the climate in Merced secures the possibilities to change supply air temperature without sacrificing the thermal comfort from humidity side. We shall implement this MPC algorithm with Lagrangian Multiplier into other environment conditions, like San Francisco and Miami. Also, if we want to apply this approach to other types of commercial building, such as

gyms, lounges, and data centers. the indoor humidity and frequency of air flow discharging will definitely need to change. Therefore, the enthalpy and humidity balance need to be involved in the air flow dynamical models and energy balance model.

The newly built buildings on UC Merced campus, Social Science and Management (SSM) Building, Student Service Building (SSB) and Science and Engineering Building II (SE2) are equipped with intelligent humidity sensors. It should be noted that CO_2 sensors are also available in the HVAC systems of these buildings. The ppm of CO_2 can be an effective index of both ventilation and thermal comfort evaluation. Similar patterns can be followed to also implement CO_2 control to the proposed method as that of humidity.

5.2.2 Online Implementation of MPC to Building HVAC Systems

We shall expand and enhance the gradient-based MPC algorithm by applying fuzzy control laws. We need to restore historic data and group them by seasonal, monthly, weekly, daily, and hourly time partition. The existing control strategies, the internal thermal load, and climate can be saved as references to the MPC algorithm. If the predicted energy consumption and thermal comfort level is not as good as the existing control laws under similar model states, we shall stick to the original control variable before.

We shall also complete the real-time building HVAC system commissioning with the proposed control strategy. Figure 5.1 shows the workflow of an online MPC of building HVAC systems. Specifically, the online receding algorithm can be divided into several steps. First, an automatic data acquisition and pre-processing module is needed. For an online user interface BAS, such as WebCTRL®, data from original sensor measurements can be collected over the web service by adopting structured information exchanging implementation, such as the Simple Object Access Protocol (SOAP). Digital filters, like Savitzky-Golay filter we used in Chapter 4, will be also designed to reduce the measurement noise. Next, data-driven models can be built from the stored data, as well as all the past operational records, internal thermal load of the office zone and climate conditions at that time. Then we apply the MPC algorithm to the real-time data by choosing right model and compute the future control input. After that, a evaluation of objective functions, like energy saving and thermal comfort will be calculated between the existing mode and the optimal control. A decision will be made to take or not take the computed control variables. At last, the control result will be recorded and the model will be updated and imposed on new data in the time domain.

We shall also develop a graphical user interface (GUI) to present the MPC objective functions and constraints in a user-friendly and informative manner. Thus, the result can be shown up. According to the real-time data trend, the MPC results

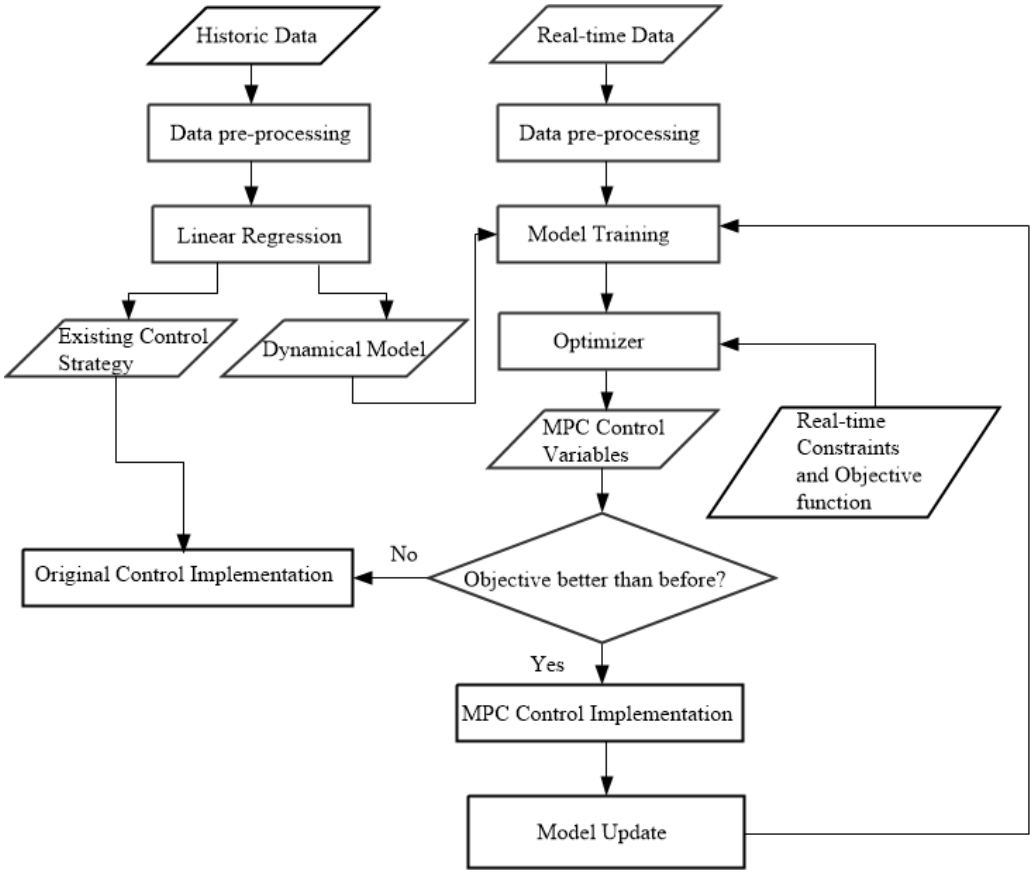

Figure 5.1: The flow chart of an MPC strategy for HVAC system with a fuzzy law.

can be analyzed and the corresponding change to MPC algorithm can be done by parameter turning on the GUI directly.

The data acquisition and pre-processing part can be realized by the SOAP module of Python. The newest version of MATLAB supports Python calls so that the data acquisition, computing, and return can be done simultaneously. For the GUI part, MATLAB Simulink works for combining desktop computing with the Internet connectivity. The implementation of the entire control strategy will involve intensive programming effort of the two language.

5.2.3 Cross-level MPC of HVAC systems

The MPC structure we have developed link VAVs to AHU. The implementation of the ARMAX model and MPC control law to AHU paves the way for local model development and control design of VAVs. The VAV is a simple version of AHU without multi-function and a Single-input, single-output system. Thus, we can follow the same procedure to build models for each VAV and apply the proposed MPC optimal algorithm to them. For each MPC, local control variables can be computed according to the room's thermal condition and occupants' demand. Then we can allow the collaboration between the MPC of AHU the lower-level MPCs. AS shown in Figure 5.2 we shall build a communication network between MPC of AHU and the distributed MPCs of VAVs. The local VAVs can send their demand of the air flow rate and cooling load, then the supply air flow rate and supply air temperature can be set to serve VAVs. Meanwhile, to keep the ventilation level and cover the cooling load simultaneously in summer, the MPC of AHU also tracks the outside air temperature and return air temperature, and determines the distribution of mixing air flow. With the return air as feedback from VAVs and outside air as disturbance, the MPC of AHU also influence the set points of discharge air flow and room temperature. That's how this cross-level MPC of HVAC systems works. In this algorithm, both global system and local system performance are taken into consideration, that is good for the trade-off between energy efficiency and thermal comfort.

We shall build an entire structure of the cross-level MPC of HVAC systems and compare the performance with those of other system-level MPC of HVAC systems, such as decentralized MPC and centralized MPC.

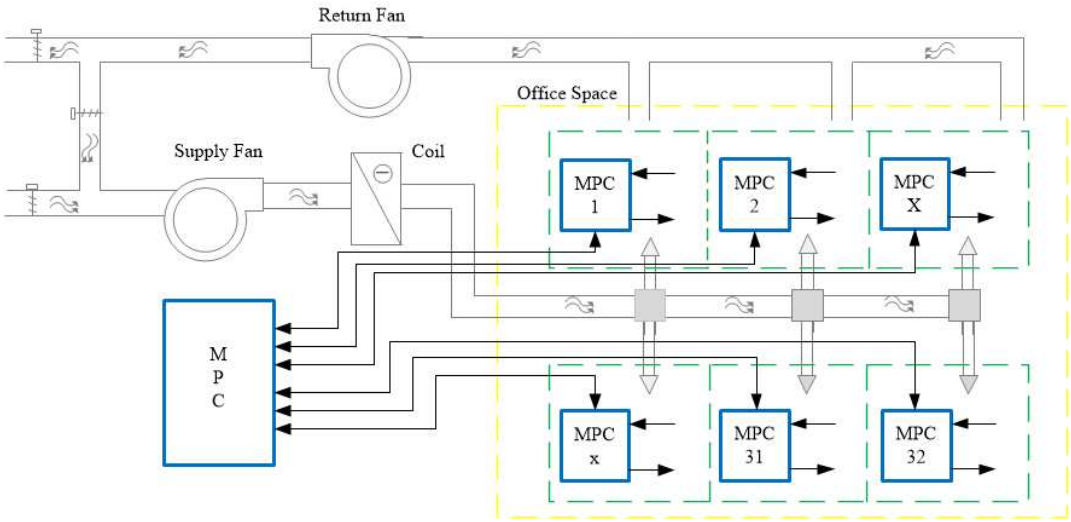

Figure 5.2: A future structure of cross-level MPC framework with a communication network.

BIBLIOGRAPHY

[1] http://www.cacx.org/meetings/meetings/2012-08-09/NBI_CCC_Webinar_080912.pdf, Fault detection & diagnostics (FDD) rooftop HVAC units: Technology, code requirements, commissioning.

[2] http://buildingsdatabook.eren.doe.gov/TableView.aspx?table=1.1.1, U.S. residential and commercial buildings total primary energy consumption (quadrillion btu and percent of total) (2011).

[3] http://buildingsdatabook.eren.doe.gov/TableView.aspx?table=1.1.3, Buildings share of U.S. primary energy consumption (percent) (2011).

[4] http://buildingsdatabook.eren.doe.gov/TableView.aspx?table=1.1.9, Buildings share of U.S. electricity consumption (percent) (2011).

[5] U. EIA, Annual energy outlook 2014, Tech. rep. (2014).

[6] A. S. ASHRAE, Standard 90.1-2004, Energy standard for buildings except low rise residential buildings, American Society of Heating, Refrigerating and Air-Conditioning Engineers, Inc.

[7] C. E. Commission, 2013 Building Energy Efficiency Standards for Residential and Nonresidential Buildings, California Energy Commission, 2013.

[8] K. I. Krakow, S. Lin, PI control of fan speed to maintain constant discharge pressure, ASHRAE Transactions-American Society of Heating Refrigerating Airconditioning Engin 101 (2) (1995) 398–407.

[9] I. Jette, M. Zaheer-Uddin, P. Fazio, PI-control of dual duct systems: manual tuning and control loop interaction, Energy conversion and management 39 (14) (1998) 1471–1482.

[10] J. Bai, S. Wang, X. Zhang, Development of an adaptive smith predictor-based self-tuning PI controller for an HVAC system in a test room, Energy and Buildings 40 (12) (2008) 2244–2252.

[11] Q. Bi, W.-J. Cai, Q.-G. Wang, C.-C. Hang, E.-L. Lee, Y. Sun, K.-D. Liu, Y. Zhang, B. Zou, Advanced controller auto-tuning and its application in HVAC systems, Control Engineering Practice 8 (6) (2000) 633–644.

[12] T. Salsbury, A survey of control technologies in the building automation industry, in: the 16th IFAC World Congress, 2005, pp. 1396–1407.

[13] D. S. Naidu, C. G. Rieger, Advanced control strategies for heating, ventilation, air-conditioning, and refrigeration systemsAn overview: Part I: Hard control, HVACR Research 17 (1) (2011) 2–21.

[14] X.-D. He, H. H. Asada, A new feedback linearization approach to advanced control of multi-unit HVAC systems, in: American Control Conference, 2003. Proceedings of the 2003, Vol. 3, IEEE, 2003, pp. 2311–2316.

[15] H. Moradi, M. Saffar-Avval, F. Bakhtiari-Nejad, Nonlinear multivariable control and performance analysis of an air-handling unit, Energy and Buildings 43 (4) (2011) 805–813.

[16] S. Wang, X. Xu, Optimal and robust control of outdoor ventilation airflow rate for improving energy efficiency and IAQ, Building and Environment 39 (7) (2004) 763–773.

[17] J. House, T. Smith, J. Arora, Optimal control of a thermal system, ASHRAE Transactions 97 (2) (1991) 991–1001.

[18] S. Wang, X. Jin, Model-based optimal control of VAV air-conditioning system using genetic algorithm, Building and Environment 35 (6) (2000) 471–487.

[19] A. Kusiak, G. Xu, Modeling and optimization of HVAC systems using a dynamic neural network, Energy 42 (1) (2012) 241–250.

[20] A. I. Dounis, C. Caraiscos, Advanced control systems engineering for energy and comfort management in a building environment-A review, Renewable and Sustainable Energy Reviews 13 (6) (2009) 1246–1261.

[21] S. A. Kalogirou, Artificial neural networks and genetic algorithms in energy applications in buildings, Advances in Building Energy Research 3 (1) (2009) 83–119.

[22] S. A. Klein, TRNSYS, a transient system simulation program, Solar Energy Laborataory, University of Wisconsin–Madison, 1979.

[23] L. Magnier, F. Haghighat, Multiobjective optimization of building design using TRNSYS simulations, genetic algorithm, and Artificial Neural Network, Building and Environment 45 (3) (2010) 739–746.

[24] J. Liang, R. Du, Thermal comfort control based on neural network for HVAC application, in: Control Applications, IEEE, 2005, pp. 819–824.

[25] D. Kolokotsa, D. Tsiavos, G. Stavrakakis, K. Kalaitzakis, E. Antonidakis, Advanced fuzzy logic controllers design and evaluation for buildings occupants thermalvisual comfort and indoor air quality satisfaction, Energy and buildings 33 (6) (2001) 531–543.

[26] S. Prívara, J. Cigler, Z. Váňa, F. Oldewurtel, C. Sagerschnig, E. Žáčeková, Building modeling as a crucial part for building predictive control, Energy and Buildings 56 (2013) 8–22.

[27] D. S. Naidu, C. G. Rieger, Advanced control strategies for heating, ventilation, air-conditioning, and refrigeration systemsAn overview: Part II: Soft and fusion control, HVACR Research 17 (2) (2011) 144–158.

[28] A. Afram, F. Janabi-Sharifi, Theory and applications of HVAC control systemsA review of model predictive control (MPC), Building and Environment 72 (2014) 343–355.

[29] J. Širokỳ, F. Oldewurtel, J. Cigler, S. Prívara, Experimental analysis of model predictive control for an energy efficient building heating system, Applied Energy 88 (9) (2011) 3079–3087.

[30] M. Maasoumy, A. Sangiovanni-Vincentelli, Total and peak energy consumption minimization of building HVAC systems using model predictive control, IEEE Design Test of Computers 29 (4).

[31] P.-D. Moroşan, R. Bourdais, D. Dumur, J. Buisson, Building temperature regulation using a distributed model predictive control, Energy and Buildings 42 (9) (2010) 1445–1452.

[32] S. Prívara, J. Širokỳ, L. Ferkl, J. Cigler, Model predictive control of a building heating system: The first experience, Energy and Buildings 43 (2) (2011) 564–572.

[33] A. Aswani, N. Master, J. Taneja, D. Culler, C. Tomlin, Reducing transient and steady state electricity consumption in hvac using learning-based model-predictive control, Proceedings of the IEEE 100 (1) (2012) 240–253.

[34] H. Lü, L. Jia, S. Kong, Z. Zhang, Predictive functional control based on fuzzy TS model for HVAC systems temperature control, Journal of Control Theory and Applications 5 (1) (2007) 94–98.

[35] G. Huang, Model predictive control of VAV zone thermal systems concerning bi-linearity and gain nonlinearity, Control Engineering Practice 19 (7) (2011) 700–710.

[36] M. Maasoumy, Comparison of control strategies for energy efficient building HVAC systems, in: ACM Symposium on Simulation for Architecture and Urban Design (SimAUD 2014), 2014.

[37] J. Rehrl, M. Horn, Temperature control for HVAC systems based on exact linearization and model predictive control, in: Control Applications (CCA), IEEE, 2011, pp. 1119–1124.

[38] H. Yoshida, S. Kumar, RARX algorithm based model development and application to real time data for on-line fault detection in VAV AHU units, IBPSA Building Simulation 99 (1999) 161–168.

[39] B. Tashtoush, M. Molhim, M. Al-Rousan, Dynamic model of an HVAC system for control analysis, Energy 30 (10) (2005) 1729–1745.

[40] P. O. Fanger, Thermal Comfort, Danish Technical Press., Copenhagen, 1970.

[41] P. O. Fanger, A. K. Melikov, H. Hanzawa, J. Ring, Air turbulence and sensation of draught, Energy and Buildings 12 (1) (1988) 21–39.

[42] American Society of Heating Refrigerating and Air Conditioning Engineers (ASHARE), Thermal Environmental Conditions for Human Occupancy (ASHARE, Standard 55-1992).

[43] International Standards Organization (ISO), Moderate Thermal Environments: Determination of the PMV and PPD Indices and Specification of the Conditions for Thermal Comfort (ISO 7730:1994).

[44] S. Wang, X. Xu, Parameter estimation of internal thermal mass of building dynamic models using genetic algorithm, Energy Conversion and Management 47 (13) (2006) 1927–1941.

[45] A. Thosar, A. Patra, S. Bhattacharyya, Feedback linearization based control of a variable air volume air conditioning system for cooling applications, ISA transactions 47 (3) (2008) 339–349.

[46] G. J. Ríos-Moreno, M. Trejo-Perea, R. Castañeda-Miranda, V. M. Hernández-Guzmán, G. Herrera-Ruiz, Modelling temperature in intelligent buildings by means of autoregressive models, Automation in Construction 16 (5) (2007) 713–722.

[47] J. C. M. Yiu, S. Wang, Multiple ARMAX modeling scheme for forecasting air conditioning system performance, Energy Conversion and Management 48 (8) (2007) 2276–2285.

[48] G. Mustafaraj, J. Chen, G. Lowry, Development of room temperature and relative humidity linear parametric models for an open office using BMS data, Energy and Buildings 42 (3) (2010) 348–356.

[49] X.-C. Xi, A.-N. Poo, S.-K. Chou, Support vector regression model predictive control on a HVAC plant, Control Engineering Practice 15 (8) (2007) 897–908.

[50] S. Wu, J. Q. Sun, A physics-based linear parametric model of room temperature in office buildings, Building and Environment 50 (2012) 1–9, DOI: 10.1016/j.buildenv.2011.10.005.

[51] S. Wu, J.-Q. Sun, Multi-stage regression linear parametric models of room temperature in office buildings, Building and Environment 56 (2012) 69–77.

[52] S. Wu, J. Q. Sun, Two-stage regression model of thermal comfort in office buildings, Building and Environment 57 (2012) 88–96.

[53] S. Wu, System-level monitoring and diagnosis of building hvac system, Ph.D. thesis, University of California, Merced (2013).

[54] D. B. Crawley, L. K. Lawrie, C. O. Pedersen, F. C. Winkelmann, Energy plus: energy simulation program, ASHRAE journal 42 (4) (2000) 49–56.

[55] T. Chow, G. Zhang, Z. Lin, C. Song, Global optimization of absorption chiller system by genetic algorithm and neural network, Energy and buildings 34 (1) (2002) 103–109.

[56] G.-Y. Jin, W.-J. Cai, L. Lu, E. L. Lee, A. Chiang, A simplified modeling of mechanical cooling tower for control and optimization of HVAC systems, Energy conversion and management 48 (2) (2007) 355–365.

[57] W. Wang, S. Katipamula, Y. Huang, M. R. Brambley, Energy savings and economics of advanced control strategies for packaged air conditioners with gas heat, Energy and Buildings 65 (2013) 497–507.

[58] Y.-W. Wang, W.-J. Cai, Y.-C. Soh, S.-J. Li, L. Lu, L. Xie, A simplified modeling of cooling coils for control and optimization of HVAC systems, Energy Conversion and Management 45 (18) (2004) 2915–2930.

[59] K. F. Fong, V. I. Hanby, T.-T. Chow, HVAC system optimization for energy management by evolutionary programming, Energy and Buildings 38 (3) (2006) 220–231.

[60] J. E. Seem, Air handling unit including control system that prevents outside air from entering the unit through an exhaust air damper (1998).

[61] G. Wang, M. Liu, Optimal outside air control for air handling units with humidity control, in: Proceedings of the 6th International Conference for Enhanced Building Operations, Shenzhen, China, 2006.

[62] S. Yuan, R. A. Perez, Model predictive control of supply air temperature and outside air intake rate of a VAV air-handling unit, ASHRAE transactions (2006) 145–161.

[63] N. Nassif, S. Moujaes, A new operating strategy for economizer dampers of VAV system, Energy and Buildings 40 (3) (2008) 289–299.

[64] N. Nassif, Performance analysis of supply and return fans for HVAC systems under different operating strategies of economizer dampers, Energy and Buildings 42 (7) (2010) 1026–1037.

[65] J. Seem, J. House, Development and evaluation of optimization-based air economizer strategies, Applied Energy 87 (3) (2010) 910–924.

[66] G. Wang, L. Song, Air handling unit supply air temperature optimal control during economizer cycles, Energy and Buildings 49 (2012) 310–316.

[67] B. A. Ogunnaike, W. H. Ray, Process Dynamics, Modeling, and Control, Vol. 9, Oxford University Press New York, 1994.

[68] M. A. Henson, D. E. Seborg, Nonlinear Process Control, Prentice-Hall, Inc., 1997.

[69] E. F. Camacho, C. B. Alba, Model Predictive Control, Springer, 2013.

[70] J. V. Candy, Signal processing: model based approach, McGraw-Hill, Inc., 1986.

[71] D. P. Bertsekas, Nonlinear Programming, 1999.

[72] P. E. Gill, W. Murray, M. H. Wright, Practical Optimization, 1981.

[73] A. E. Bryson, Applied Optimal Control: Optimization, Estimation and Control, CRC Press, 1975.

[74] K. Zhou, J. C. Doyle, K. Glover, Robust and Optimal Control, Vol. 40, Prentice Hall New Jersey, 1996.

[75] K. R. Muske, J. W. Howse, G. A. Hansen, Lagrangian solution methods for nonlinear model predictive control, in: American Control Conference, 2000. Proceedings of the 2000, Vol. 6, IEEE, 2000, pp. 4239–4243.

[76] P. TøNdel, T. A. Johansen, A. Bemporad, An algorithm for multi-parametric quadratic programming and explicit MPC solutions, Automatica 39 (3) (2003) 489–497.

[77] M. Hovd, Multi-level programming for designing penalty functions for MPC controllers, in: Proceedings of the 18th IFAC World Congress, 2011, pp. 6098–6103.

[78] S. Richter, M. Morari, C. N. Jones, Towards computational complexity certification for constrained MPC based on lagrange relaxation and the fast gradient method, in: Decision and Control and European Control Conference (CDC-ECC), IEEE, 2011, pp. 5223–5229.

[79] V. Nedelcu, I. Necoara, Iteration complexity of an inexact augmented lagrangian method for constrained MPC, in: Decision and Control (CDC), 2012, pp. 650–655.

[80] G. Knabe, C. Felsmann, Optimal operation control of HVAC systems, in: Proceedings of 5th IBPSA Conference, 1997.

[81] L. Marletta, A comparison of methods for optimizing air-conditioning systems according to the exergonomic approach, Journal of energy resources technology 123 (4) (2001) 304–310.

[82] Y.-C. Chang, A novel energy conservation methodoptimal chiller loading, Electric Power Systems Research 69 (2) (2004) 221–226.

[83] A. Kelman, F. Borrelli, Bilinear model predictive control of a HVAC system using sequential quadratic programming, in: IFAC World Congress, 2011.

[84] S. T. Bushby, BACnetTM: a standard communication infrastructure for intelligent buildings, Automation in Construction 6 (5).

[85] http://www.automatedlogic.com/product/webctrl/, Webctrl®(2014).

[86] Q. Bi, W.-J. Cai, E.-L. Lee, Q.-G. Wang, C.-C. Hang, Y. Zhang, Robust identification of first-order plus dead-time model from step response, Control Engineering Practice 7 (1) (1999) 71–77.

[87] S. ASHRAE, Standard 62.12010, Ventilation for Acceptable Indoor Air Quality, ASHRAE.

[88] D. Watkins, Fundamentals of Matrix Computations, John Wiley Sons, 1991.

[89] S. Wang, J.-B. Wang, Robust sensor fault diagnosis and validation in HVAC systems, Transactions of the Institute of Measurement and Control 24 (3) (2002) 231–262.

[90] Z. Hou, Z. Lian, Y. Yao, X. Yuan, Data mining based sensor fault diagnosis and validation for building air conditioning system, Energy Conversion and Management 47 (15) (2006) 2479–2490.

[91] A. Savitzky, M. J. Golay, Smoothing and differentiation of data by simplified least squares procedures, Analytical chemistry 36 (8) (1964) 1627–1639.

[92] S. J. Orfanidis, Introduction to Signal Processing, Prentice-Hall, Inc., 1995.

[93] R. W. Schafer, What is a Savitzky-Golay filter? Signal Processing Magazine, IEEE 28 (4) (2011) 111–117.

[94] S. Butterworth, On the theory of filter amplifiers, Wireless Engineer 7 (1930) 536–541.

[95] G. Bianchi, R. Sorrentino, Electronic filter simulation design, McGraw-Hill, 2007.

[96] D. K. Lindner, Introduction to signals and systems, McGraw-Hill, 1999.

[97] C. Marquardt, N. Mai, A computational procedure for movement analysis in handwriting, Journal of neuroscience methods 52 (1) (1994) 39–45.

[98] H. Guo, M. Yu, J. Liu, J. Ning, Butterworth low-pass filter for processing inertial navigation system raw data, Journal of surveying engineering 130 (4) (2004) 175–178.

[99] G. Christodoulakis, K. Busawon, N. Caplan, S. Stewart, On the filtering and smoothing of biomechanical data, in: Communication Systems Networks and Digital Signal Processing (CSNDSP), 2010 7th International Symposium on, IEEE, 2010, pp. 512–516.

[100] C. Moler, Numerical Computing with MATLAB, Revised Reprint Edition, The Society for Industrial and Applied Mathematics, Philadelphia, 2004.

[101] H. U. Frausto, J. G. Pieters, J. M. Deltour, Modelling greenhouse temperature by means of auto regressive models, Biosystems Engineering 84 (2) (2003) 147–157.

[102] T. W. Anderson, The Statistical Analysis of Time Series, Reprint Edition, Wiley-Interscience, 1994.

[103] D. R. Brillinger, Time Series: Data Analysis and Theory, Society for Industrial and Applied Mathematics, 2001.

[104] M. Norgaard, O. Ravn, N. K. Poulsen, L. K. Hansen, Neural Networks for Modeling and Control of Dynamic Systems, Springer-Verlag, 2000.

[105] U. Norlén, Estimating thermal parameters of outdoor test cells, Building and Environment 25 (1) (1990) 17–24.

Appendix A

NOMENCLATURE

β	recirculation air ratio
ρ	Air density (kgm^{-3})
k	Time sequence of measurements
m	Control horizon
$\dot{m}$	Mass flow rate (kgs^{-1})
p	Prediction horizon
λ, μ	Lagrange Multipliers
$x(k+n \mid k)$	Expected value of $x(k+n)$ with measurement up to instant k
AHU	Air handling unit
C_p	Specific heat capacity of air ($kJkg^{-1}K^{-1}$)
CW	cooling coil
D	Damper position (%)
En	Energy Consumption (kJ)
H	Specific enthalpy ($kJkg^{-1}$)
$HVAC$	Heating, ventilation, and air conditioning
J	Objective function
MPC	Model Predictive Control
Q	Weighting factor of quadratic functions
R	Weighting factor of control penalties
T	Temperature (K)
V	Volume of room (m^3)
VFD	Variable frequency drive
W	Power of fan (kW)
Φ	Nonlinear objective function
X	An attribute
VAV	Variable air volume unit
Subscripts	
EA	exhaust air
MA	mixing air
OA	outside air
RA	return air
RF	return fan

SA	supply air
SF	supply fan
d	designed
f	air flow rate
t	temperature
rm	room
sp	set point
dis	discharge
ref	reference
$zone$	building zone